AD-A159 079 COUPLED HIGH POWER WAVEGUIDE LASER RESEARCH(U) UNITED TECHNOLOGIES RESEARCH CENTER EAST HARTFORD CT L A NEWMAN ET AL. 30 JUL 85 UTRC/R85-926869 1/1

UNCLASSIFIED AFOSR-TR-85-0734 F49620-84-C-0062 F/G 20/5 NL

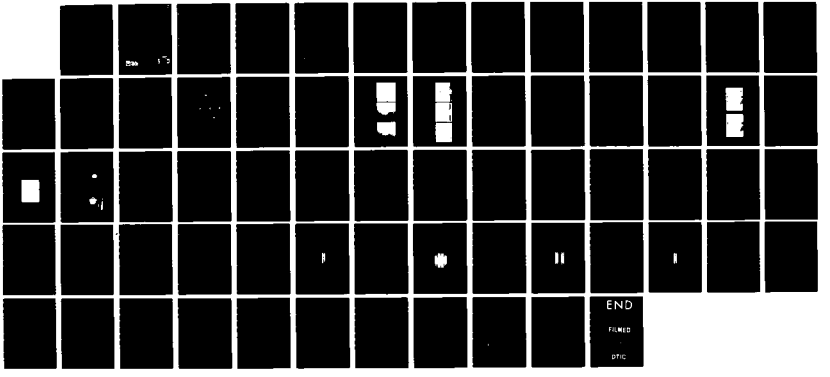

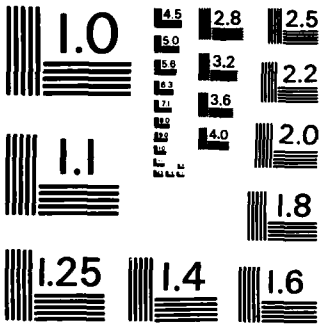

R85-926869

AFOSR-TR- 85-0734

COUPLED HIGH POWER WAVEGUIDE LASER RESEARCH

Prepared by
L.A. Newman
A.J. Cantor
R.A. Hart
J.T. Kennedy
A.J. DeMaria

Final Report
July 30, 1985

Sponsored by the Department of the Air Force
Under Contract F49620-84-C-0062

UNITED TECHNOLOGIES RESEARCH CENTER
EAST HARTFORD, CONNECTICUT 06108

Unclassified

SECURITY CLASSIFICATION OF THIS PAGE

AD-A159079

REPORT DOCUMENTATION PAGE

1a. REPORT SECURITY CLASSIFICATION: Unclassified	1b. RESTRICTIVE MARKINGS: None
2a. SECURITY CLASSIFICATION AUTHORITY	3. DISTRIBUTION/AVAILABILITY OF REPORT: Approved for public release; distribution unlimited. Unlimited Distribution
2b. DECLASSIFICATION/DOWNGRADING SCHEDULE	
4. PERFORMING ORGANIZATION REPORT NUMBER(S): R85-926869	5. MONITORING ORGANIZATION REPORT NUMBER(S): AFOSR-TR- 85-0734
6a. NAME OF PERFORMING ORGANIZATION: United Technologies Research Center; 6b. OFFICE SYMBOL (If applicable):	7a. NAME OF MONITORING ORGANIZATION: Same as 8a
6c. ADDRESS (City, State and ZIP Code): United Technologies Research Center, Silver Lane, East Hartford, CT 06108	7b. ADDRESS (City, State and ZIP Code): Same as 8c
8a. NAME OF FUNDING/SPONSORING ORGANIZATION: Air Force Office of Scientific Research; 8b. OFFICE SYMBOL (If applicable): NP	9. PROCUREMENT INSTRUMENT IDENTIFICATION NUMBER: F49620-84-C-0062
8c. ADDRESS (City, State and ZIP Code): USAF, AFSC, Building 410, Bolling AFB, DC 20332	10. SOURCE OF FUNDING NOS.

PROGRAM ELEMENT NO.	PROJECT NO.	TASK NO.	WORK UNIT NO
61102F	2301	A1	N/A

11. TITLE (Include Security Classification): (Unclassified) Coupled High Power Waveguide Laser Research

12. PERSONAL AUTHOR(S): Leon A. Newman, Arnold J. Cantor, Richard A. Hart, John T. Kennedy and Anthony J. DeMaria

13a. TYPE OF REPORT	13b. TIME COVERED	14. DATE OF REPORT (Yr., Mo., Day)	15. PAGE COUNT
Final	FROM 6/1/84 TO 5/31/85	July 30, 1985	57

16. SUPPLEMENTARY NOTATION

17. COSATI CODES			18. SUBJECT TERMS (Continue on reverse if necessary and identify by block number)
FIELD	GROUP	SUB. GR	

19. ABSTRACT (Continue on reverse if necessary and identify by block number)

See Reverse Side

20. DISTRIBUTION/AVAILABILITY OF ABSTRACT	21. ABSTRACT SECURITY CLASSIFICATION
UNCLASSIFIED/UNLIMITED ☒ SAME AS RPT ☒ DTIC USERS ☐	Unclassified

22a. NAME OF RESPONSIBLE INDIVIDUAL	22b. TELEPHONE NUMBER (Include Area Code)	22c. OFFICE SYMBOL
Howard Schlossberg	(202) 767-4908	NP

DD FORM 1473, 83 APR EDITION OF 1 JAN 73 IS OBSOLETE.

Unclassified

SECURITY CLASSIFICATION OF THIS PAGE

Block 19

The United Technologies Research Center (UTRC) conducted a research program to explore a unique ridged waveguide technique to phase-lock an array of coupled CO_2 wavequide lasers. The motivation for this investigation was to scale the output power capability of CO_2 waveguide lasers by one to two orders of magnitude greater than the present state-of-the-art (i.e., scale to power levels of 100 W to 1 kW) while maintaining single frequency operation. A one year program was conducted to test the feasibility of the ridged waveguide coupling technique.

The feasibility study clearly produced positive results. In particular, stable phase-locked operation of two and three-channel arrays was demonstrated at the 50 W level. Phase-locking was maintained in a laboratory environment for many hours without adjustments other than length tuning of the laser. In addition, a first-order theory was developed to strengthen the understanding of the coupled waveguide laser array.

R85-926869

Coupled High Power Waveguide Laser Research

TABLE OF CONTENTS

LIST OF FIGURES

LIST OF FIGURES (Cont'd)

LIST OF TABLES

Coupled High Power Waveguide Laser Research

1.0 INTRODUCTION

Since June 1, 1984, United Technologies Research Center (UTRC), under sponsorship of the Air Force Office of Scientific Research Contract No. F49620-84-C-0062, has been conducting a research program to explore a unique ridge waveguide technique for phase-locked arrays of coupled waveguide lasers. The motivation for investigating coupled waveguide laser arrays is to scale their output power by one to two orders of magnitude greater than the present state-of-the-art (i.e., scale to power levels of 100 W to 1 kW) while maintaining single frequency operation. A one year program was proposed to test the feasibility of the ridged waveguide coupling technique.

As is fully described in Section 2.0, the feasibility study has clearly produced positive results. In particular, stable phase-locked operation of two and three-channel arrays has been demonstrated at the 50 W level. Phase locking was maintained in a laboratory environment for many hours without adjustments other then length tuning of the laser. In addition, a first-order theory has been developed to help strengthen the understanding of the coupled waveguide laser array.

The first year program addressed the possibility of combining the coupled ridged waveguide concept as conceived by Dr. A. J. DeMaria and Dr. W. Bridges (Refs. 1 and 2) and RF excited CO_2 waveguide laser technology developed over the past eight years at UTRC to power combine and phase lock an array of waveguide lasers. It was envisioned that the coupled waveguide approach could provide high power transmitters for long-range laser radars on either space-based or airborne platforms.

The general concept of coupled ridge waveguides and the technique used to create an RF excited discharge within the ridged waveguides are illustrated in Figs. 1 and 2. Figure 1 illustrates the cross section of a three-element waveguide array in which the waveguides are formed by grinding slots into a ceramic slab and then placing this ceramic slab between RF electrodes. Optical coupling between the guides is achieved by shortening the ridge between the waveguide elements to form a gap with dimension "a". The amount of optical coupling

FIG. 1

RIDGED WAVEGUIDE ARRAY

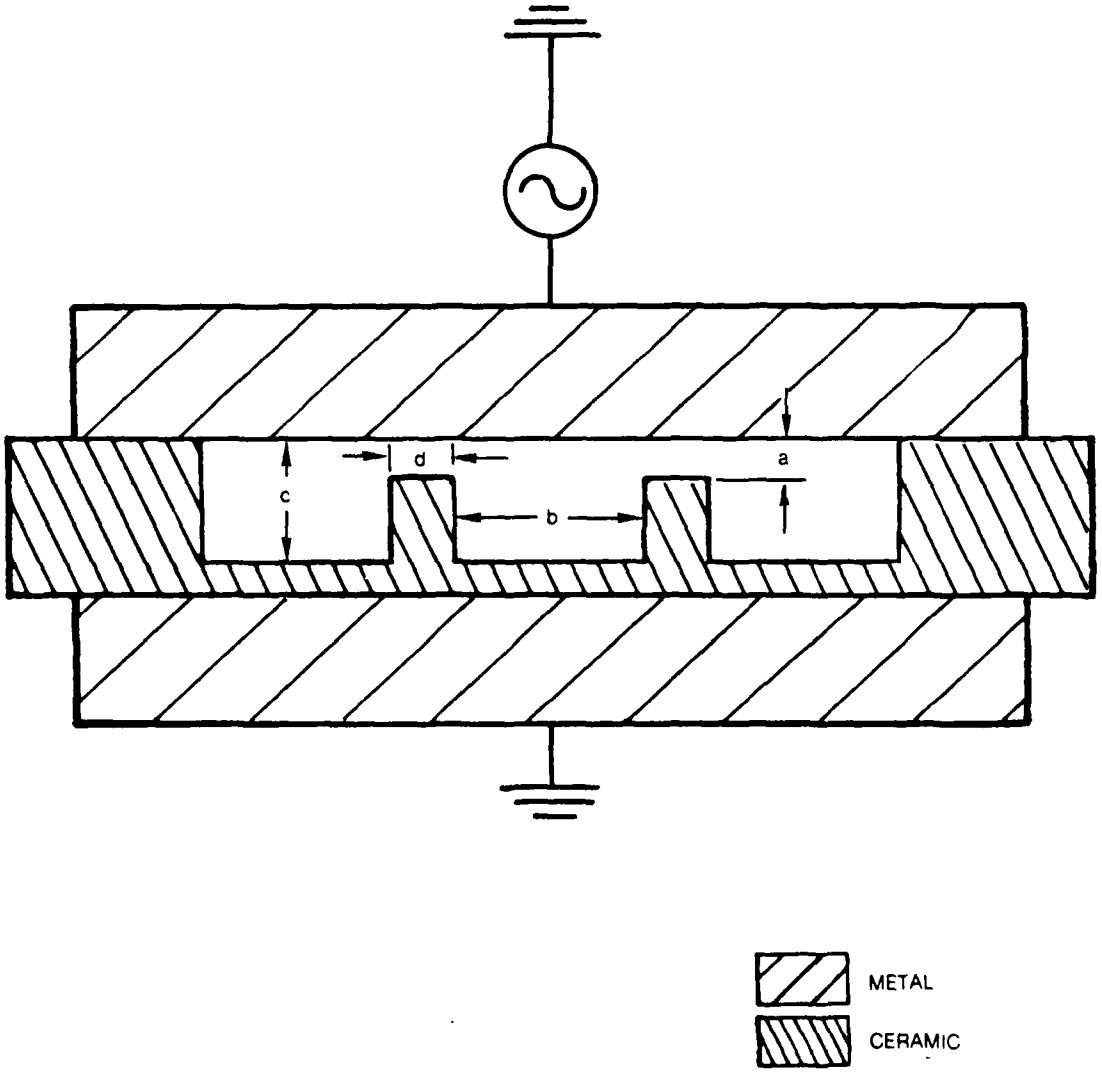

83-9-84-12

UTRC RF EXCITATION CIRCUIT COMBINED WITH A RIDGED WAVEGUIDE

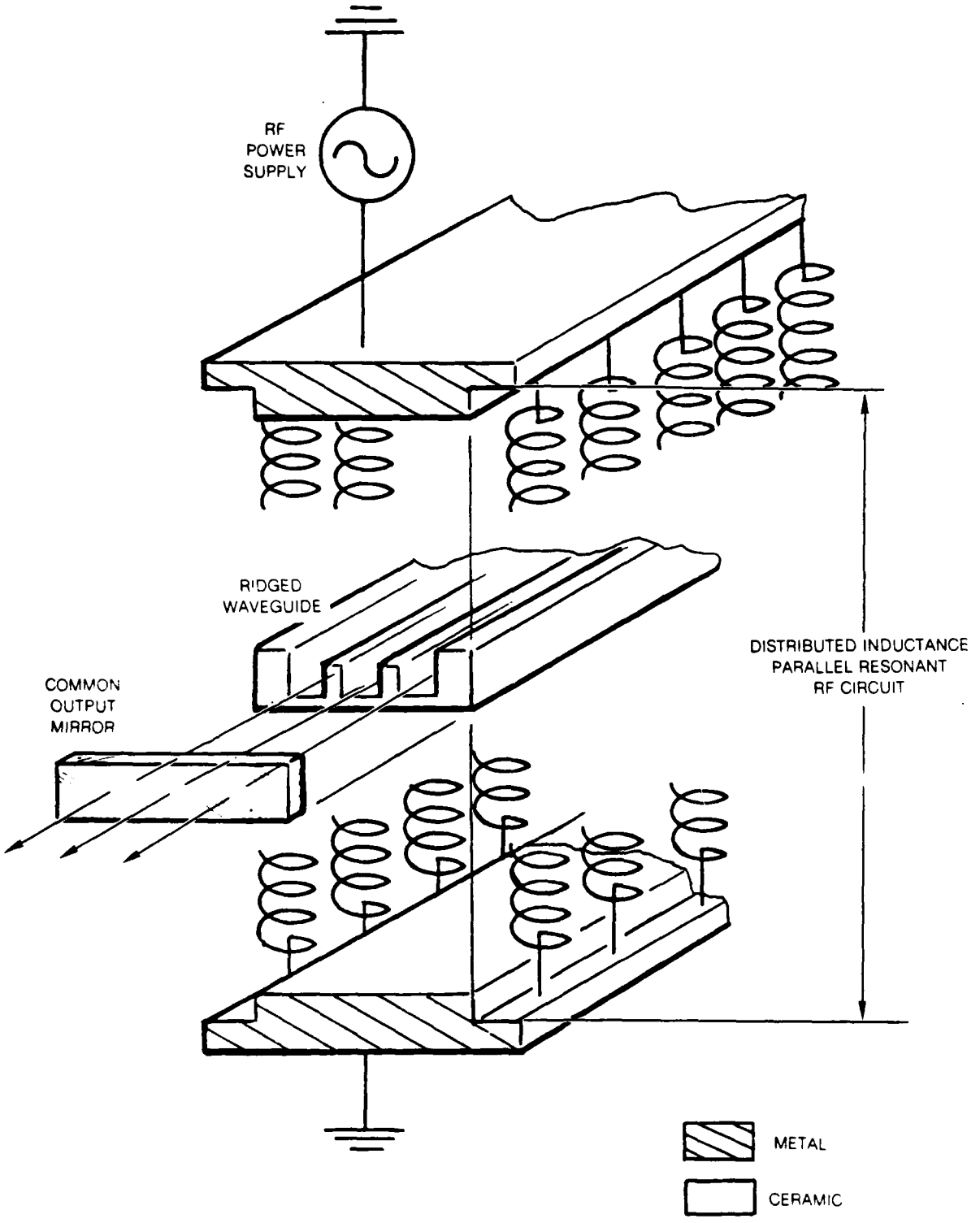

83-9-84-3

between adjacent channels is controlled by adjusting both the gap dimension "a" and the separation "d" between the channels. Dimensions "b" and "c" are equal and typically between 1 mm and 3 mm. Figure 2 illustrates how the ridged waveguide concept is combined with the UTRC RF-excitation circuit. The operation of the distributed inductance parallel resonant RF circuit is described fully in Refs. 3 and 4. The coupled waveguide resonator is formed by placing a flat common output mirror and a flat common total reflector within a few mm of each end of the waveguide laser.

In addition to the ridged waveguide concept, a diffraction coupling concept, as illustrated in Fig. 3, was also investigated during the program. With diffraction coupling, radiation from one waveguide element is coupled to its nearest neighbors by fabricating a diffraction region at one end of the waveguide array, thus mixing the individual waveguide radiators through diffraction spreading. By adjusting the length of the diffraction region and the separation between waveguide elements, the degree of coupling between the channels can be controlled.

The objective of the program was to test the feasibility of the above excitation and coupling concepts to determine if they are compatible with high power, single frequency, efficient operation. Furthermore, an effort to achieve a fundamental understanding of the parameters which control the operation of coupled waveguide lasers was to be initiated during the program by formulating a theoretical model and conducting a parametric study. In Section 2.0 the experimental effort is summarized and in Section 3.0 the theoretical effort is summarized.

FIG. 3

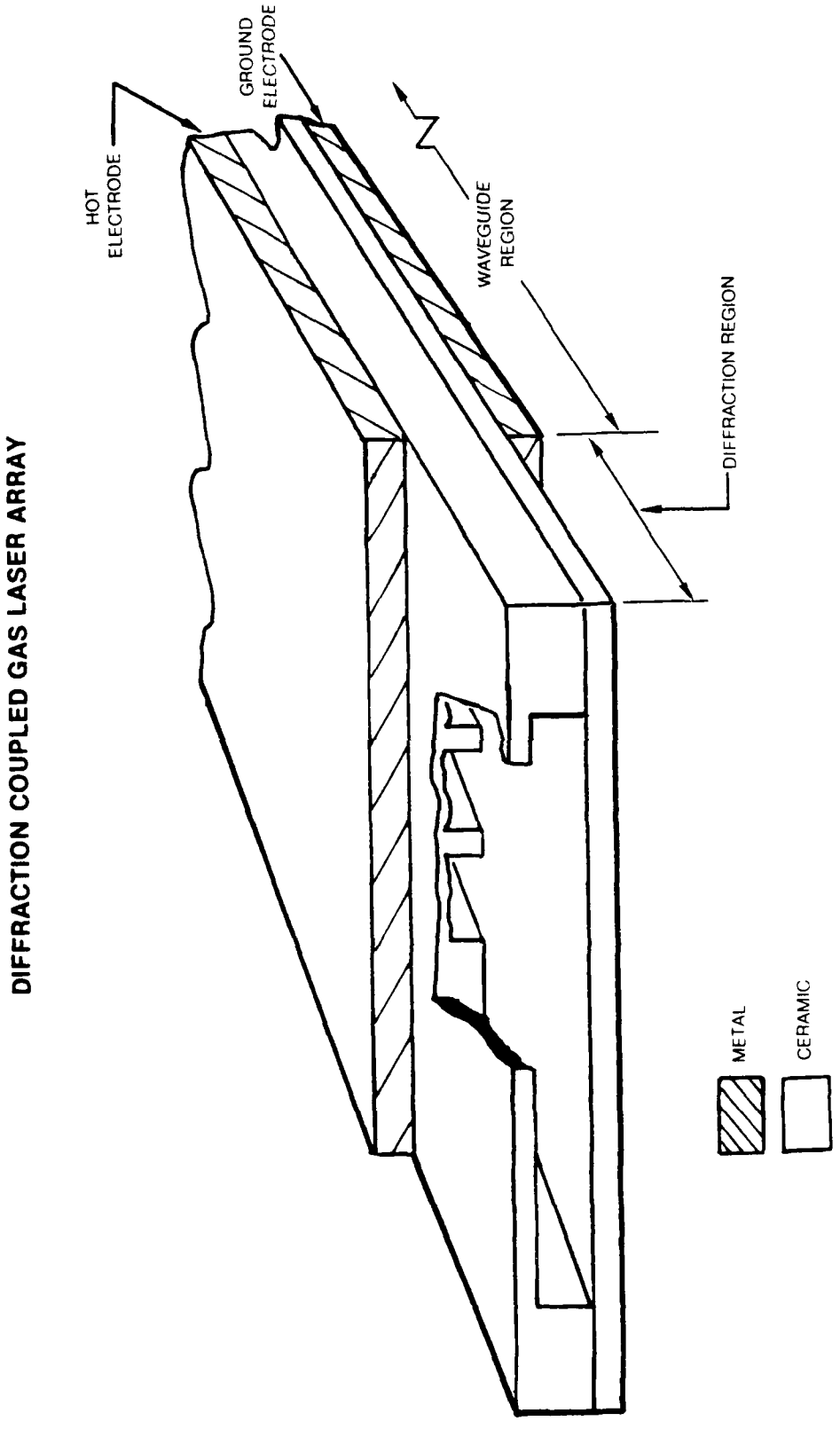
DIFFRACTION COUPLED GAS LASER ARRAY
HOT ELECTRODE
GROUND ELECTRODE
WAVEGUIDE REGION
DIFFRACTION REGION
METAL
CERAMIC
83-9-84-10

lower than the corresponding two-element waveguide, suggesting that there will not be a rapid decrease in the locking range as the number of array elements is increased. The photograph to the right shows the detector's output spectrum under locked conditions. It is to be noted that the low level RF signals evident in Fig. 13 were a result of pick-up and were not generated by the phase locked beam.

Figure 14 shows a beam scan of the three element waveguide output obtained with the galvanometer scanner and the pyroelectric detector. The beam scans shown in Fig. 14 are for phase-locked and unlocked conditions. As will be described in Section 3.0 the three-lobed mode with the intense central peak is characteristic of the phase-locked mode in which the electric fields in each channel are in phase. As expected, the on-axis intensity decreases substantially when the output mirror is adjusted to unlock the laser array.

Figure 15 presents the mode shapes for the three-channel coupled waveguide laser obtained with the IR imaging plates, together with the laser output power, RF input power, and dimensional characteristics of the waveguide. Under phase-locked operation, the in-phase mode was the only mode that was observed.

The maximum output power obtained with the three element array was 55 watts. This is well below the maximum of 75 watts expected for this configuration operating as an uncoupled waveguide laser. Clearly a major portion of this difference is a result of the RF power supply which was limited to an output power of 500 W. At this point in time, the ultimate power generating capability of the three-element array is not known. To explore the ultimate power generating limitations of this and larger arrays will require the use of more powerful RF supplies.

2.4 Mode Observations

During the course of the parametric study, observations were made of the phase-locked mode character as a function of the coupled waveguide geometry. Table 1 summarizes these observations. The waveguide geometry is defined by its type (either U-channel or square channel), number of channels, separation between channels, and the size of the coupling gap. The mode observations were characterized by the operating mode which was either symmetric (E-fields in-phase) or anti-symmetric (E-fields 180° out-of-phase) and the relative strength of the mode. Very strong means that the indicated mode was the only observed mode; strong means that the indicated mode was clearly dominant but that the other phase locked mode was also observed; weak means that the indicated mode was marginally dominant. The overall point to be made concerning the observations summarized in Table 1 is that the dominant phase-locked mode appears to be

COUPLED WAVEGUIDE LASER RESEARCH — THREE-CHANNEL LASER

SPECTRUM OF BEAT FREQUENCY DETECTOR

UNLOCKED

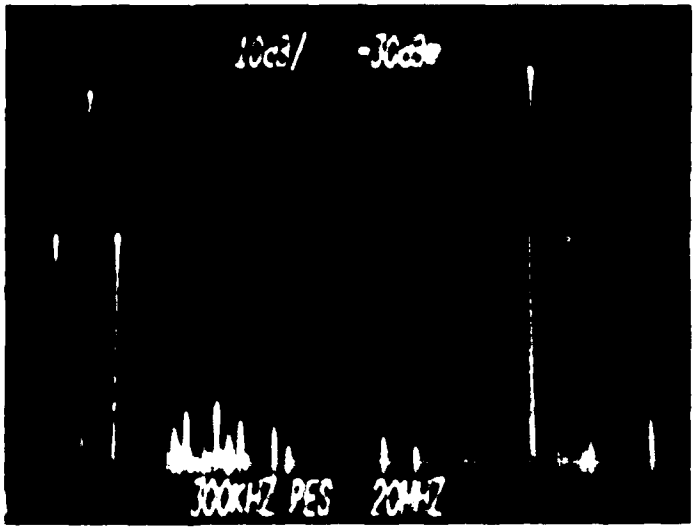

MIN BEAT
FREQUENCY = 9 MHz

R F
DRIVE

LOCKED

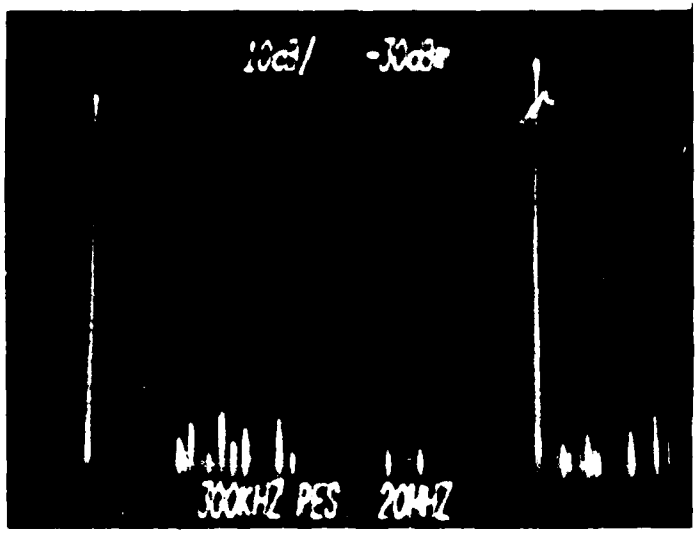

R.F
DRIVE

*NOTE LOW LEVEL SIGNAL WERE PRESENT WITH DETECTOR INPUT BLOCKED

GAP = 0.045 in. SEPARATION = 0.010 in

FIG. 12

COUPLED WAVEGUIDE LASER RESEARCH — TWO-CHANNEL EXPERIMENT

MINIMUM BEAT FREQUENCY VS SEPARATION

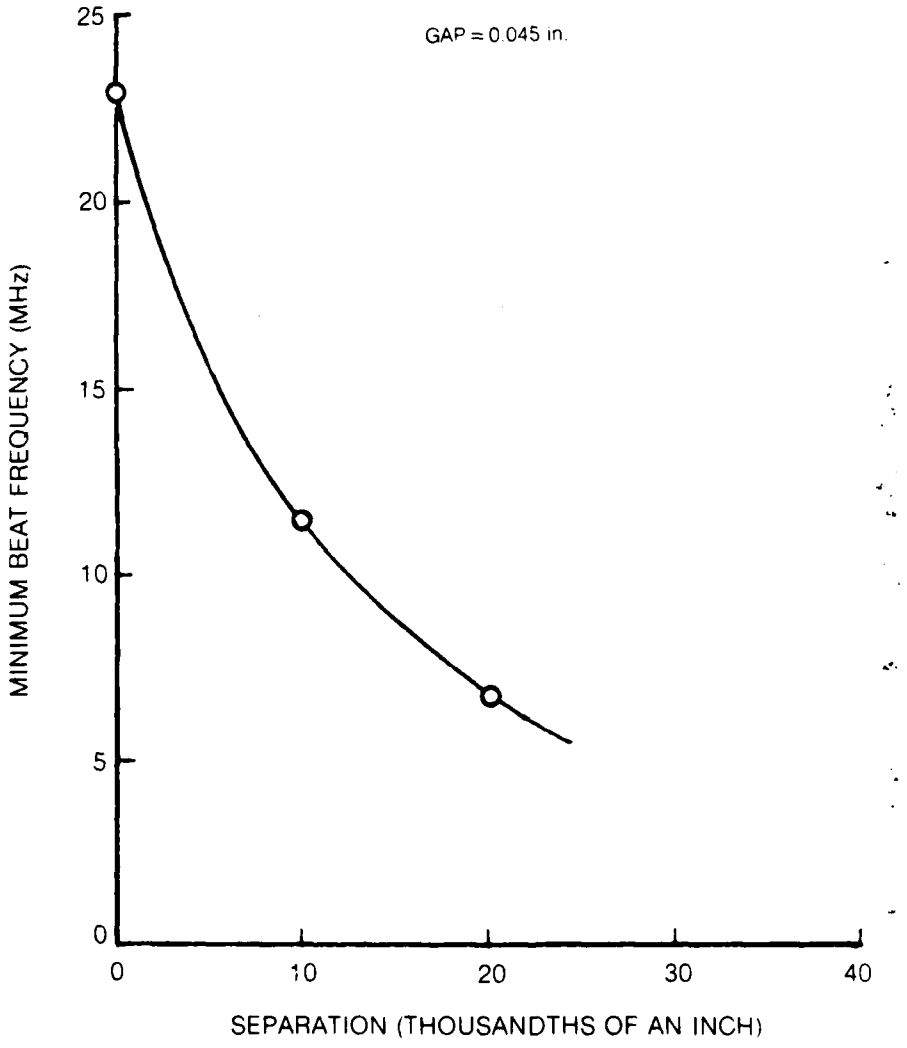

85-3-11-10

FIG. 11

COUPLED WAVEGUIDE LASER RESEARCH — TWO-CHANNEL EXPERIMENT

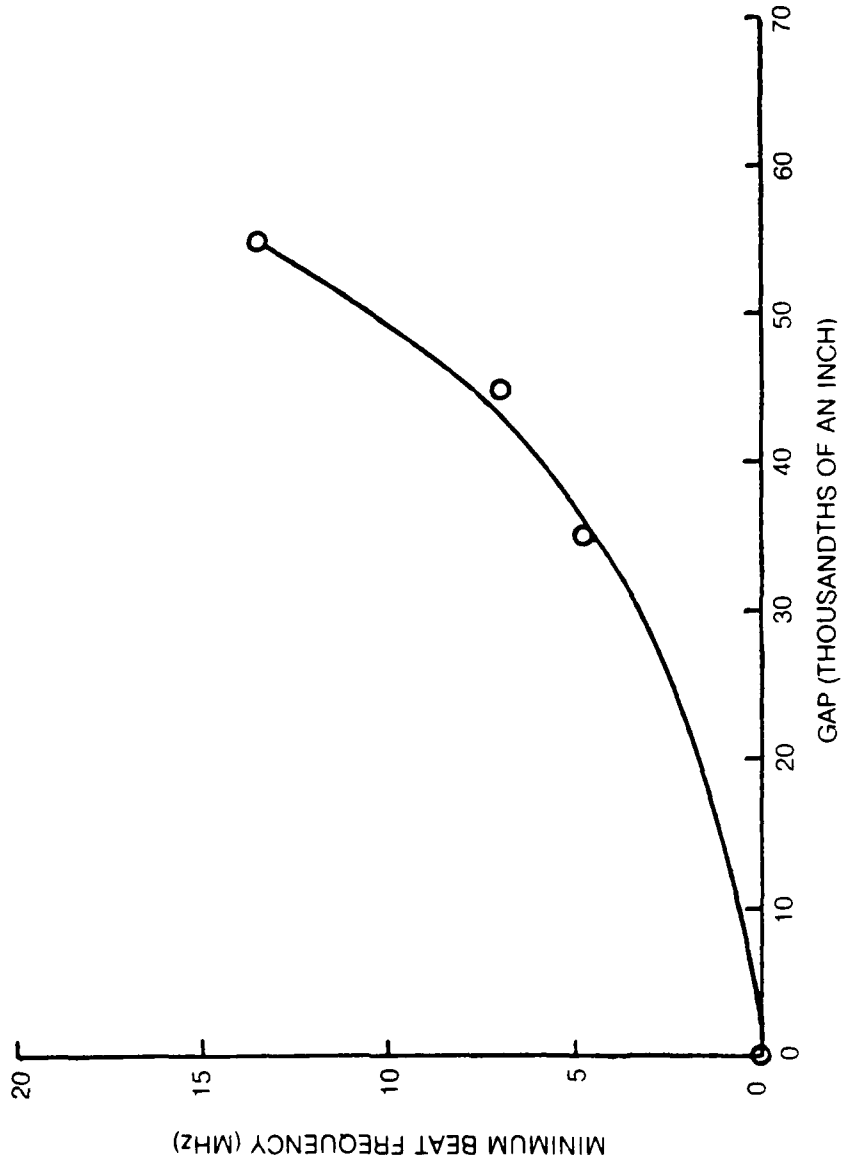

85-3-11-9

per waveguide element would be expected if they were operated separately. Thus fifty watts of output power would be expected if there was no degradation in performance of a two element array. Under the condition of zero gap, Fig. 10 shows that 50 watts of output power is obtained indicating that there is no loss in output power due to the close proximity of the two laser elements. As the gap size is increased from zero to 0.045", the output power monotonically decreases to approximately 85% of full power. Although this small amount of power loss is undesirable, it is not catastrophic. Thus, the results of this experiment indicate that the coupled ridged waveguide is compatible with high optical extraction efficiency even for a gap size of approximately 1/2 the base size.

The observed minimum beat is related to the locking range. A larger minimum beat frequency correspond to a larger locking range which in turn corresponds to a more stable laser. Because the locking range is controlled by the amount of coupling between the laser channels, geometric parameters controlling the amount of coupling such as the gap and separation dimensions would be expected to control the locking range and minimum observed beat frequency. Figure 11 presents the results of a parametric experiment in which the minimum beat frequency was recorded as a function of the gap dimension with a constant separation. Likewise, Fig. 12 presents the minimum beat frequency versus the separation with a constant gap. As would be expected, increasing the gap and decreasing the separation results in an increase in the minimum beat frequency. Figure 12 also shows that minimum beat frequencies in the 10 MHz region were routinely achieved. This explains the observed stability of the phased locked laser in the laboratory environment in which external de-stabilizing forces such as temperature fluctuations and vibration have previously been measured to result in relative frequency fluctuation between the waveguide elements in the 100 kHz region (well below the 10 MHz region).

In addition to the ridged waveguide coupling technique, a few experiments were conducted with the diffraction coupling technique. In order to achieve stable phase locking with this technique it was found necessary to remove a 4 cm length of the wall separating the two waveguide elements on both ends of the waveguide. Unfortunately under this condition, the output power droped from 50 W to only 25 W. It therefore appears that this technique is not compatible with high optical extraction efficiency as is the ridged waveguide coupling technique.

2.3 Three Channel Experiment

One three channel waveguide was fabricated and tested with bore, gap and separation dimensions of 0.090", 0.045", and 0.010" respectively. Figure 13 shows the frequency spectrum of the high-speed detector's output. The left-hand spectrum shows that a minimum beat of 9 MHz was achieved. This is only 2 MHz

FIG. 10

COUPLED WAVEGUIDE LASER RESEARCH — TWO-CHANNEL EXPERIMENT

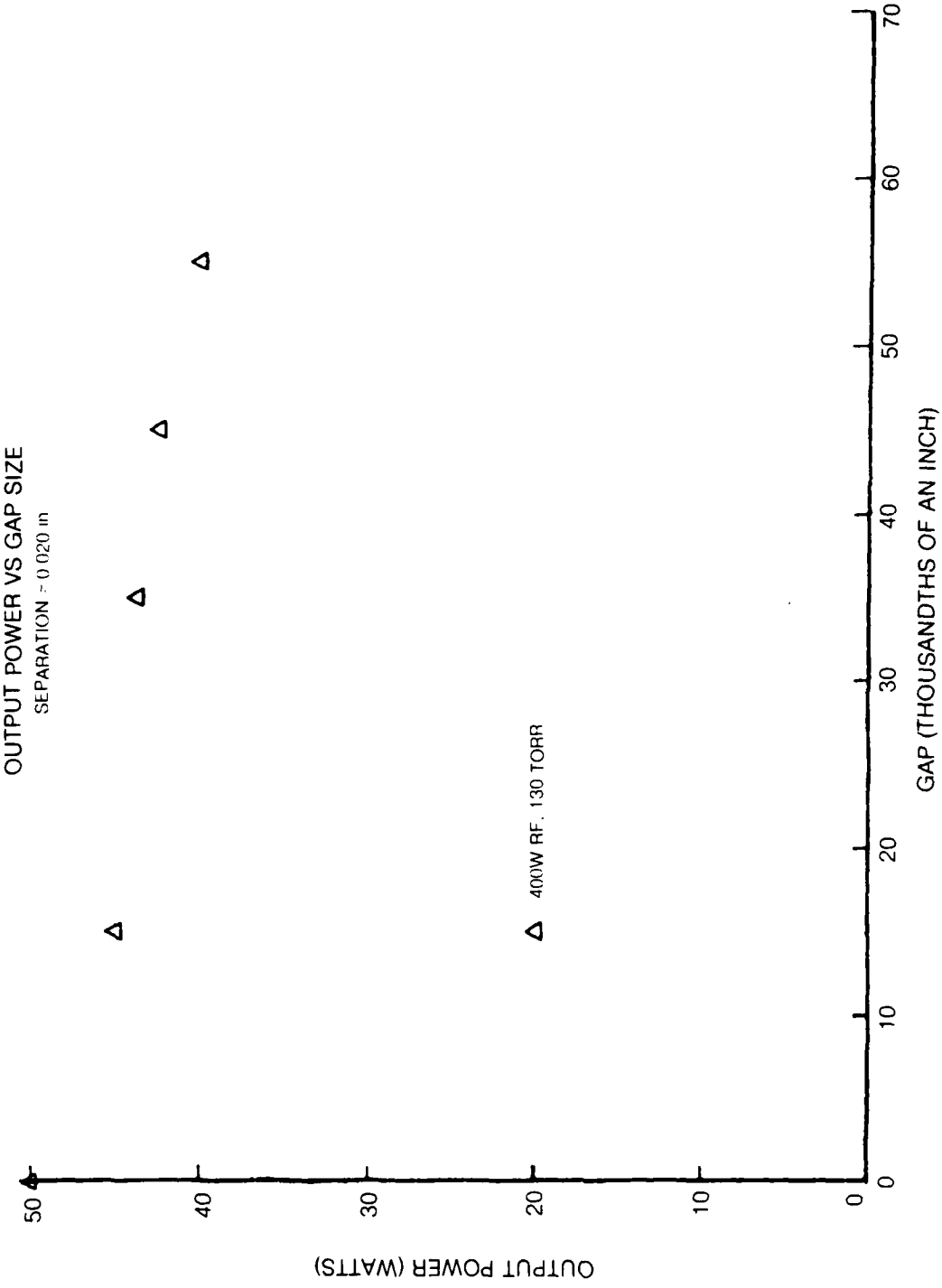

85-3-11-8

DUAL CHANNEL COUPLED WAVEGUIDE LASER

(FAR-FIELD INTENSITY SCAN)

LASER OUTPUT POWER = 47 W
GAIN LENGTHS = 37 cm
GAP = 0.045 in.

RF INPUT POWER = 425 W
SEPARATION = 0.010 in.
BORE DIAMETER = 0.090 in.

100μv/div

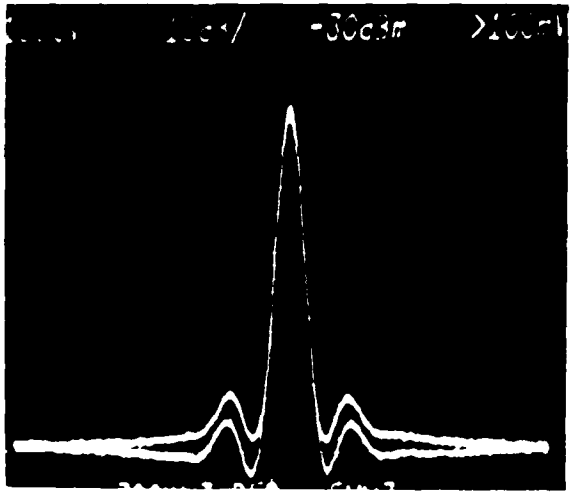

PHASE-LOCKED SYMMETRIC

50μv/div

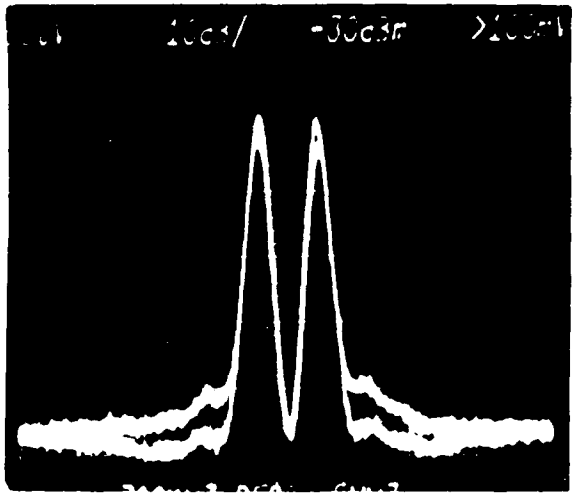

PHASE-LOCKED ANTI-SYMMETRIC

50μv/div

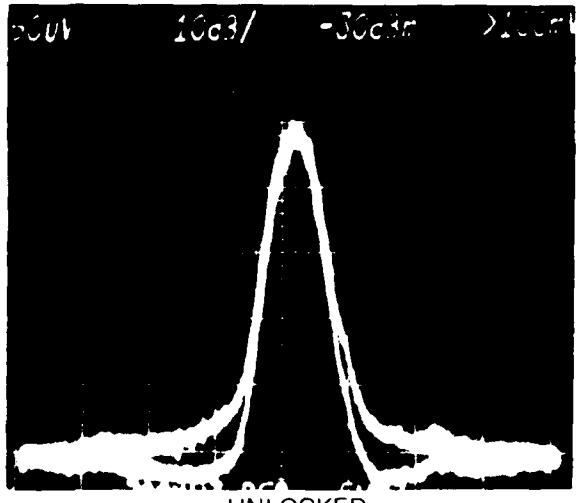

UNLOCKED

DUAL-CHANNEL COUPLED WAVEGUIDE LASER

FAR-FIELD INTENSITY PATTERN

LASER OUTPUT POWER = 47 w
RF INPUT POWER = 425 w
GAIN LENGTH = 37 cm
SEPARATION = 0.010 in.
BORE DIAMETER = 0.090 in.
GAP = 0.045 in.

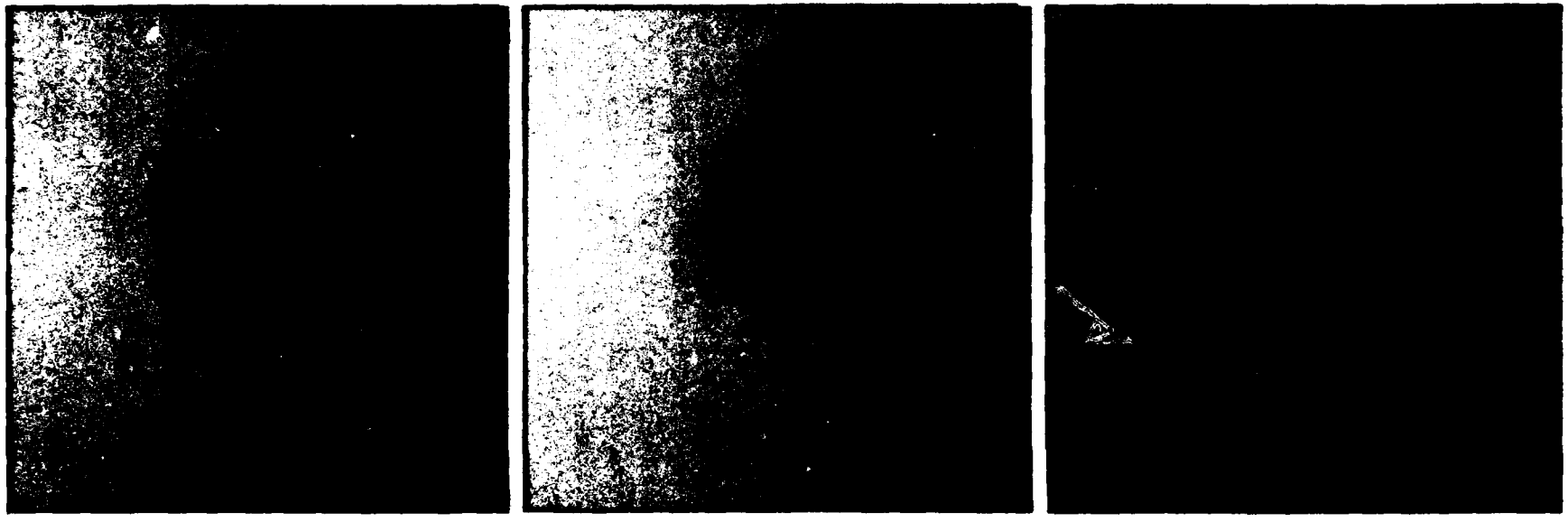

PHASE-LOCKED SYMMETRIC | PHASE-LOCKED ANTI-SYMMETRIC | UNLOCKED

greater, the on-axis intensity was nearly independent of the beat frequency. As the beat frequency was adjusted to approximately 11 MHz, a rapid increases in the on-axis intensity occurred. Just below 11 MHz, the beat frequency vanished indicating single frequency phase locked operation and the on-axis intensity was maximized.

In conjunction with the on-axis intensity data, IR imaging plates were used to display far-field mode patterns such as are shown in Fig. 8. Under the condition of beating between the waveguide elements (i.e., the unlocked condition) the mode appeared as a round spot. This pattern is that expected when two Gaussian beams close together are incoherently mixed in the far-field. When the mirror tilt is adjusted such that phase locking is obtained and the on-axis intensity is maximized, the phase locked symmetric mode pattern shown in Fig. 8 was obtained. In this case the electric fields in the two waveguide elements are in phase and therefore produce an on-axis intensity maximum in the far-field. By further adjusting the tilt for this particular waveguide geometry, the phase-locked anti-symmetric mode was also observed, as shown in the center photograph of Fig. 8. In this case the electric fields in the two waveguide elements are 180° out-of-phase and therefore produce an on-axis null in the far-field. When the mirror tilt was adjusted for phase-locked operation, phase locking could be maintained for hours with only a length adjustment of the cavity via the PZT mirror mount. The above results clearly demonstrate that stable phase-locked operation of a coupled ridged waveguide array is feasible.

Figure 9 presents the beam intensity profile for the symmetric, anti-symmetric, and unlocked modes as measured by scanning the beam back and forth across an apertured pyroelectric detector. The dual trace evident in each of the beam scans is caused by differences in the measured beam profile in one scan direction relative to the measured beam profile in the opposite scan direction and is an artifact of the pyroelectric detector. Note that the sensitivity of the anti-symmetric, and unlocked scans is 2 times greater than the sensitivity of the symmetric mode. For this data it is seen that the ratio of the peak intensity of the symmetric mode to that of both the anti-symmetric mode and the unlocked mode is approximately a factor of two. This measured result agrees with the theoretical prediction to be discussed in Section 3.0. The discrepancy between the factor of ~ 2 obtained from the data presented in Fig. 9 and the factor of ~ 1.5 presented in Fig. 7 was found to be caused by using too large an aperture to measure the on-axis intensity for the data of Fig. 7.

The next issue addressed by the first year program was whether high optical extraction efficiency could be achieved with a coupled ridged waveguide array. To address this issue, a set of experiments were conducted in which the output power of the array was measured as a function of the gap size for a fixed separation of 0.020". The results of this experiment are shown in Fig. 10. Under the mixture, pressure and pump conditions for this experiment, approximately 25 watts

COUPLED WAVEGUIDE LASER RESEARCH — TWO-CHANNEL EXPERIMENT

ON-AXIS INTENSITY VS BEAT FREQUENCY

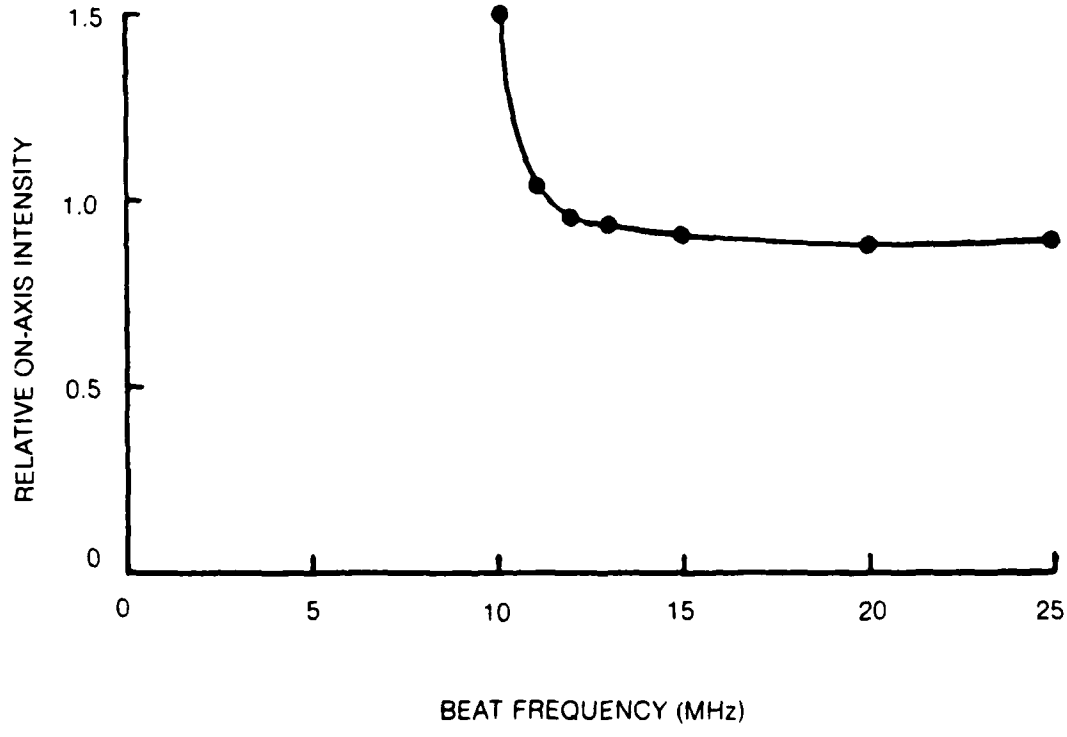

85-3-11-6

FIG. 6

DIAGNOSTIC CONFIGURATION FOR FEASIBILITY STUDY

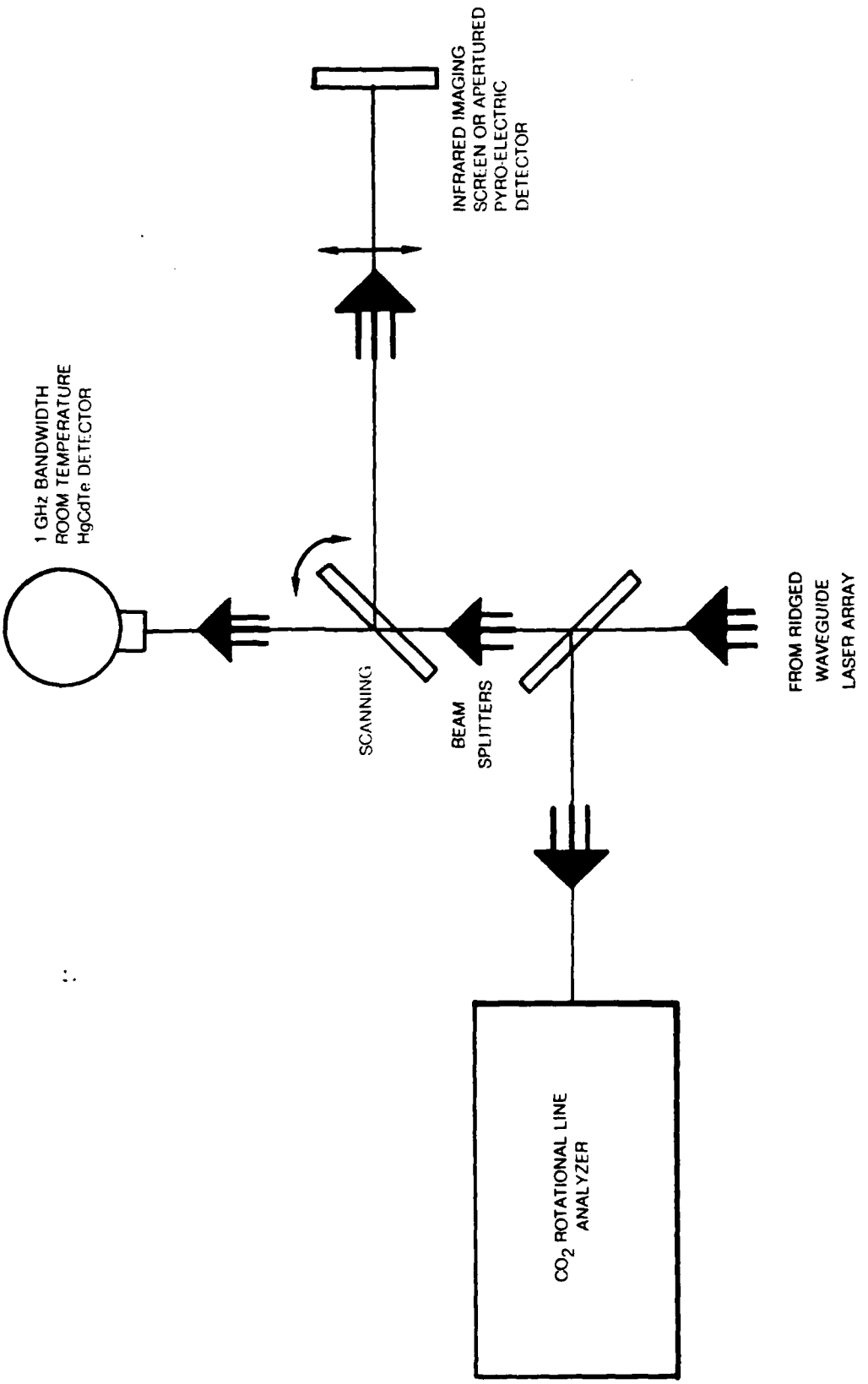

83-9-84-14

FIG. 5

OPTICAL CAVITY CONFIGURATION FOR FEASIBILITY STUDY

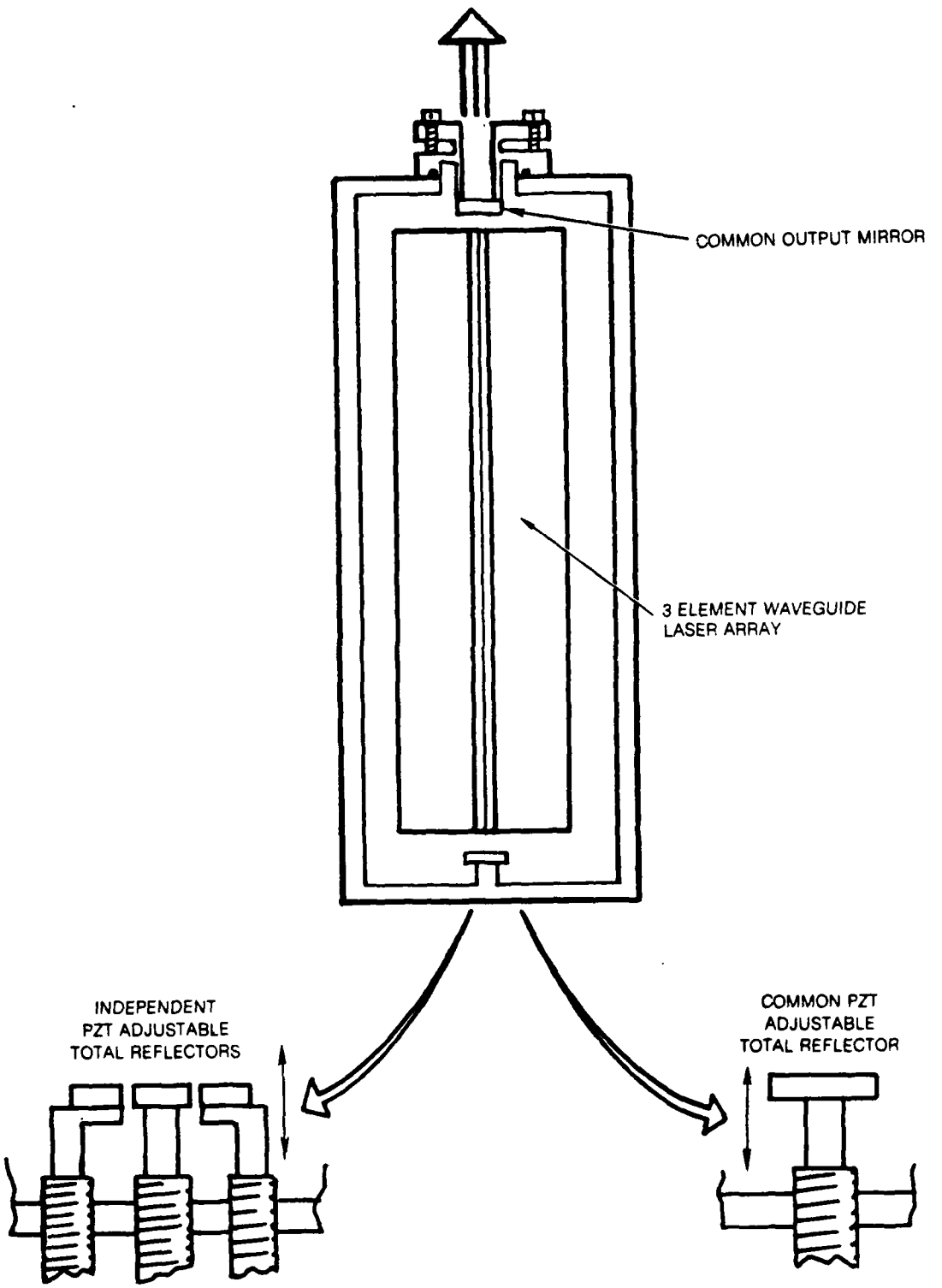

83-9-84-13

EXPERIMENTAL SET-UP COUPLED WAVEGUIDE LASER RESEARCH

WAVEGUIDE CONFIGURATIONS

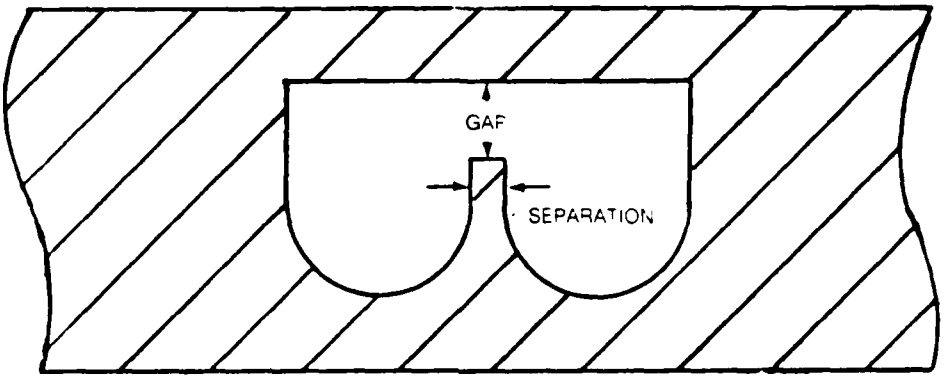

U-CHANNEL

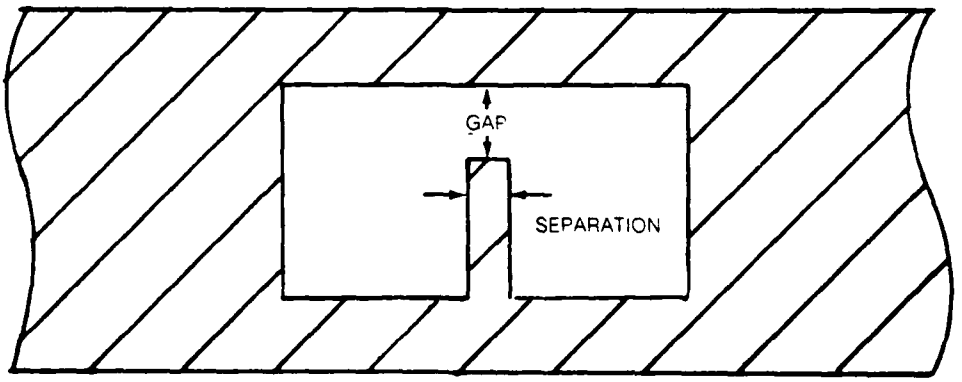

SQUARE-CHANNEL

85-3-11-7

2.0 EXPERIMENTAL EFFORT

2.1 Experimental Set-Up

Figure 4 shows the waveguide configurations used during the feasibility program. The U-channel configuration permitted very small waveguide separation to be achieved; in fact, zero separation between the channels could be achieved. On the other hand, the square-channel configuration was limited to separations greater than 0.010" because of the lack of support near the base of the ridge.

Figure 5 shows the optical cavity configuration for the feasibility study which consists of a common output mirror, a waveguide laser array, and a PZT-adjustable total reflector. Both independently adjustable and commonly adjustable end mirrors were fabricated. However, alignment difficulties were encountered with the independently-adjustable mirror concept and therefore no actual experiments were conducted with this configuration.

Figure 6 illustrates the diagnostic configuration used during the feasibility study. A sample of the laser array output was obtained with a beam splitter and propagated to a spectrometer. The spectrometer was used to monitor the lasing rotational transition(s) of the laser array. A second beam splitter was used to generate another beam sample which propagated to either an infrared imaging screen or a single element pyroelectric detector with an aperture of 0.5 mm. The second beam splitter was mounted on a galvanometer scanner thus permitting the laser output to be scanned across the pyroelectric detector to produce beam intensity profiles. The portion of the beam transmitted through the second beam splitter was incident on a fast photoconductive detector. By monitoring the beat frequency between the elements of the laser array, it could be determined whether the laser was operating in a single-frequency locked condition, or in a multi-frequency unlocked condition.

2.2 Two Channel Experiments

Before conducting experiments with three element arrays, experiments were conducted with two-element arrays to reduce the complexity of the experiment and simplify the interpretation of the experimental results.

Initial experiments concentrated on demonstrating that phased locked operation of two-element coupled ridge waveguides could be achieved. Figure 7 presents the on-axis intensity of a two-element array as a function of the beat frequency between the array elements. For this experiment, the bore diameter, separation, and gap dimension were 0.090", 0.010" and 0.045" respectively. The beat frequency between the two waveguide elements was adjusted by adjusting the tilt of the output mirror. At beat frequencies of approximately 12 MHz and

FIG. 14

COUPLED WAVEGUIDE LASER RESEARCH — THREE-CHANNEL LASER

PHASE LOCKED FAR-FIELD BEAM PROFILE

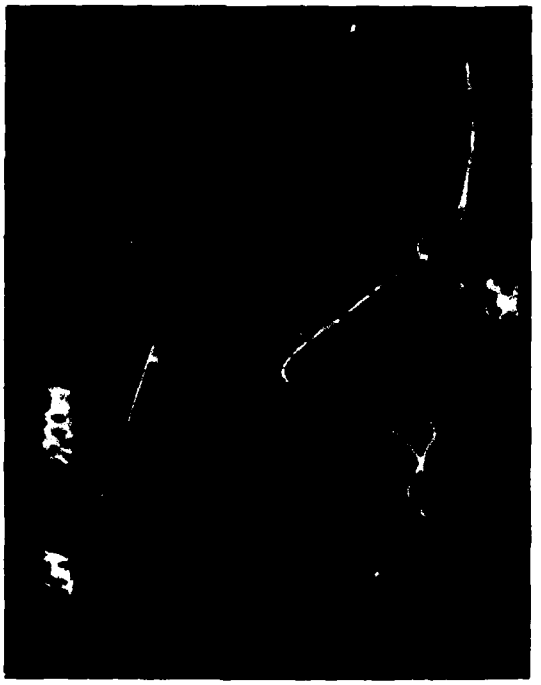

85-3-11-12

THREE-CHANNEL COUPLED WAVEGUIDE LASER

FAR-FIELD INTENSITY PATTERN

LASER OUTPUT POWER = 55w
RF INPUT POWER = 500 + w
GAIN LENGTH = 37 cm
SEPARATION = 0.010 in.
BORE DIAMETER = 0.090 in.
GAP = 0.045 in.

PHASE-LOCKED

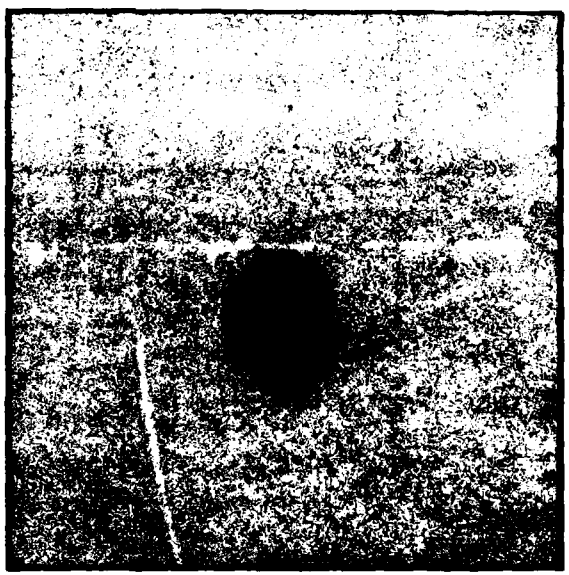

UNLOCKED

TABLE 1
COUPLED WAVEGUIDE RESEARCH — MODE OBSERVATIONS

- DOMINANT MODE VS WAVEGUIDE GEOMETRY

WAVEGUIDE GEOMETRY				DOMINANT MODE	RELATIVE STRENGTH
TYPE	# OF CHANNELS	SEPARATION	GAP		
U	2	0	0.045	ANTI-SYMMETRIC	VERY STRONG
U	2	0	0.055	ANTI-SYMMETRIC	VERY STRONG
U	2	0.010	0.045	SYMMETRIC	STRONG
U	2	0.020	0.035	ANTI-SYMMETRIC	WEAK
U	2	0.020	0.045	ANTI-SYMMETRIC	WEAK
U	2	0.020	0.055	ANTI-SYMMETRIC	WEAK
SQUARE	2	0.013	0.030	ANTI-SYMMETRIC	VERY STRONG
U	3	0.010	0.045	SYMMETRIC	VERY STRONG

dependent upon the waveguide geometry. However, the theory as presently formulated does not show dependence of the dominant mode on the details of the waveguide geometry. Thus it must be concluded that the factors which control the dominant phase locked mode are not understood.

Another observation was that as the gap size increased beyond 0.045", the tendency for multi-mode (multi-frequency) operation increased substantially. In the case of the 0.055" gap size, single-frequency operation was difficult to achieve. Qualitatively, the normal output from waveguide arrays with a 0.055" gap size appeared to be 90% in the single-frequency phase-locked mode with the remaining 10% of the power in higher-order modes at different frequencies. These observations suggest that the gap size should be limited to approximately 1/2 the bore size or less.

3.0 THEORETICAL EFFORT

3.1 Introduction

The goal of theoretical analysis of the coupled waveguide laser geometries is to explain the following:

1) Conditions under which phase-locking is possible;
2) Extent of the locking-range;
3) Stability of the phase-locked state;
4) Far-field beam shape and intensity when phase-locked; and, of course,
5) Agreement or disagreement of theory and experiment.

It was not possible, within the limitations of the present program, to analyze the experiments in their full detail. Nor is it fully established how to do this when the coupling of the lasers is strong. However, it was possible to formulate the equations for a first-order theory of coupled waveguides, corresponding to a condition of weak coupling, and to solve these equations in special cases which permit one to begin analyzing the experiments. These results will be discussed in succeeding sections. Here we will just present a brief overview of the results.

The equations of the first-order theory, known as Coupled-Mode Theory, assume that each one of the N coupled waveguide lasers is operating in its usual low-order mode, and that the coupling between the lasers only affects the amplitudes and phases attributed to each laser. The amplitudes and phases will adjust themselves to produce self-consistent patterns which have come to be known in the semiconductor coupled-laser area as supermodes. If the equations for the system of coupled lasers are reduced to linear equations, their solutions are just the well-known normal-modes of coupled oscillators. The basic theoretical result for this problem is that: for N oscillators there are N normal modes, each one distinguished by a unique frequency, and a unique set of amplitudes and phases. When non-linear terms are put back into the equations, such as those describing the gain and saturation due to the lasing medium, the theoretical problem becomes much more difficult. For certain kinds of nonlinear terms, however, there are new effects which are not included in the linear effects. With linear equations, any linear combination of solutions (such as the normal-modes) is also a solution. With nonlinear equations, one can have mode suppression (one mode supresses all the others), and mode-locking (the beat frequencies between pairs of modes lock to a common value) in one laser, and phase-locking (the amplitudes and phases of different lasers lock together in certain preferred combinations). Since we have assumed one mode per laser, our main interest is in phase-locking.

In Section 3.2 we present the results for the normal modes of coupled waveguide resonators, i.e. neglecting the lasing medium in the lasers. We provide only a few of the basic equations, and concentrate on the results of the analysis. These results include predictions for the far-field beam patterns associated with the normal modes. Qualitative agreement with thermal beam patterns and swept intensity profiles is good. But numerical agreement with ratios of measurements of peak intensities is not very good. This may be due to inadequacies in the experimental arrangement; for example, the range at which the intensity profiles are measured may not be sufficient to ensure being in the far-field. However, perfect agreement is not expected for two reasons: (1) the strength of the coupling is probably too great for the weak-coupling assumption to be valid; and (2) the nonlinear terms have been neglected. As far as (1) is concerned, the coupled-mode theory does not predict the magnitude of the coupling parameter, nor does it give any indication of how small it should be. One has to carry out detailed mode calculations for the actual geometry, or at least for simpler but comparable geometeries, in order to calculate the magnitude of the coupling constant; and one must estimate the contribution of higher-order modes in order to judge the strength of the coupling. As far as (2) is concerned, the linear-theory modes can be solutions in the presence of non-linear laser effects provided certain restrictions are imposed on the small-signal gains (or on the losses) of the individual lasers. These restrictions were not imposed, and the nonlinear equations have not yet been solved in detail.

One task that will require further research is to solve the nonlinear equations for the phase-locked solutions. Experimentally, a phase-locked state does exist, and so a solution for the weak-coupling case is expected to exist, even if it is not accurate in detail. Section 3.3 discusses the phase-locking equations. Two results of further analysis are expected: (1) changes to the linear-theory predictions for amplitudes and phases; and (2) calculation of the locking-range. The locking-range is observed experimentally by changing the length of one laser resonator, or (equivalently) its waveguide frequency, relative to the lengths (or frequencies) of the others. Within a certain range of frequency differences, the lasers will all be locked-up in one of the supermodes. Once the mismatch in resonator frequencies reaches a certain level, the lasers break lock, and the nice phased-array features of the far-field beam are lost. The extent of the mismatch tolerated by phase-locking, which depends on the magnitude of the coupling constant, determines how stable the phase-locked state is to vibrations, thermal expansion, and other environmental variations. In addition, the experimental results with a variety of channel separations and coupling gap widths show that the supermode in which the lasers naturally lock-up is not always the preferred symmetric mode, and that the sensitivity of the locked-up mode to mirror adjustments seems to depend on geometry. No theoretical results are yet available to explain these new observations.

3.2 Coupled-Mode Theory Results

Figure 16 summarizes the status of theoretical modeling for the purposes of the coupled waveguide program. The modes of hollow dielectric waveguides (before lasing action is included) are known in the literature for square, rectangular, and circular cross-sections. They are not known for the U-shaped cross-section; however, our experiments show that the U-shaped channel is just as effective as the square channel for fabricating a highly-efficient waveguide laser.

The double-channel rectangular waveguide with a partition has been treated in the microwave literature under the name of ridged waveguide. Results exist in the form of series solutions, including series transcendental equations for determining the frequencies of the modes. These can be evaluated numerically. The double-channel rectangular waveguide with an infinitely-thin partition is a special case of the ridged waveguide, and is also a good model to study for the coupling of U-shaped channels because of the vanishingly-thin partition edge which is possible with this configuration. The double-U-shaped waveguide may require other methods of solutions, but the modes of the single U-shaped channel will be required for them.

It is known that the lowest-order mode for each of the calculable guides has the lowest loss per unit length. Hence, when lasing it is the lowest-order mode which is established. The modes of the rectangular hollow dielectric guide, neglecting small terms, have the shape of sine and cosine functions in both transverse directions, as indicated in Fig. 17 (Ref. 5). If the modal 'quantum numbers' m or n are odd integers, one is required to take the cosine function; if m or n are even integers, one takes the sine function. The effect, in either case, is that (to the approximation indicated) the electric and magnetic fields that are not identically zero everywhere within the guide are zero on all of the boundary walls. When a rectangular channel is operated as a laser, the field distribution in the cavity, as well as that of the emerging beam, consists of the product of two cosine curves which are zero at the ends and a maximum in the center.

When a gap is opened in the wall separating two channels, a new distribution of electromagnetic fields develops, but for a small gap the fields in each of the two channels are expected to, and do, closely resemble the fields with no gap. In this case, the lowest-order modes are still an accurate representation for the fields. The residual effect of the coupling produced by the gap is that the amplitudes and phases of the fields in the two channels become coupled, which is consistent with the overall conservation of energy. This limit of weakly-coupled lasers is formally similar to many classical problems, such as the problem of coupled pendulums indicated in Fig. 18.

STATUS OF THEORETICAL MODELING

- SINGLE CHANNEL

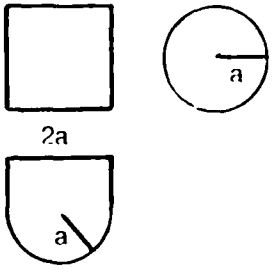

HOLLOW DIELECTRIC WAVEGUIDES
- MODES ARE KNOWN

MIXED GEOMETRY
- MODES NOT KNOWN

- DOUBLE CHANNEL

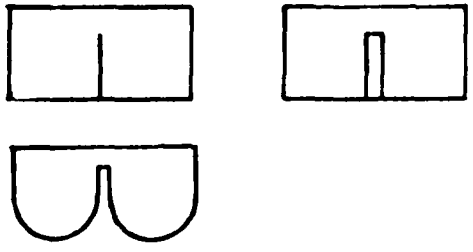

RIDGED WAVEGUIDES
- SERIES-SOLUTIONS DERIVED FOR THIN PARTITION
- CALCULATIONS NEEDED FOR THICK PARTITION

- MODES NOT KNOWN, NEW METHOD NEEDED

- COUPLED-MODE ANALYSIS

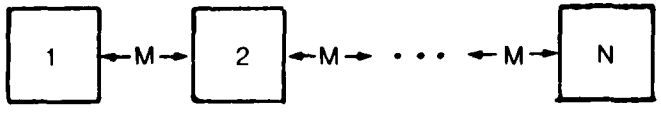

FORMALISM DEVELOPED FOR WEAK COUPLING
- M UNKNOWN, NEED NORMAL-MODES
- LOCKING-RANGE TO BE CALCULATED

WAVEGUIDE LASER MODES

Hybrid Modes $E^yH^x_{mn}$ $(m, n \geq 1)$

$$E_y = \begin{Bmatrix} \cos\left(\frac{m\pi x}{2a}\right) \\ \sin\left(\frac{m\pi x}{2a}\right) \end{Bmatrix} \begin{Bmatrix} \cos\left(\frac{n\pi y}{2b}\right) \\ \sin\left(\frac{n\pi y}{2b}\right) \end{Bmatrix} e^{i(\gamma_{mn} z - \omega t)}$$

$$H_x = -\sqrt{\frac{\epsilon_0}{\mu_0}}\, E_y$$

$$H_z = 0\left(\frac{\lambda}{a}\right)$$

$$E_x = 0\left(\frac{\lambda}{b}\right),$$

$$\beta_{nm} = \mathrm{Re}\{\gamma_{nm}\} = k\left\{1 - \frac{1}{2}\left[\left(\frac{m\pi}{2ka}\right)^2\left(1 - \frac{2}{ka}\,\mathrm{Im}\left\{\frac{1}{\sqrt{v^2-1}}\right\}\right) + \left(\frac{n\pi}{2kb}\right)^2\left(1 - \frac{2}{kb}\,\mathrm{Im}\left\{\frac{v^2}{\sqrt{v^2-1}}\right\}\right)\right]\right\}$$

and

$$\alpha_{nm} = \mathrm{Im}\{\gamma_{nm}\} = \frac{\pi^2}{4k^2}\left[\frac{m^2}{a^3}\,\mathrm{Re}\left\{\frac{1}{\sqrt{v^2-1}}\right\} + \frac{n^2}{b^3}\,\mathrm{Re}\left\{\frac{v^2}{\sqrt{v^2-1}}\right\}\right],$$

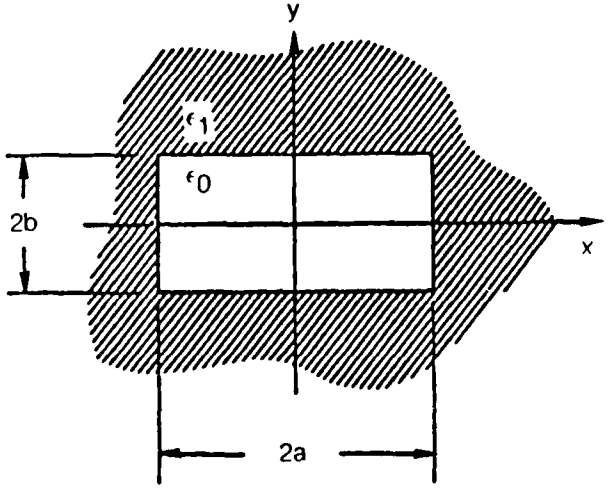

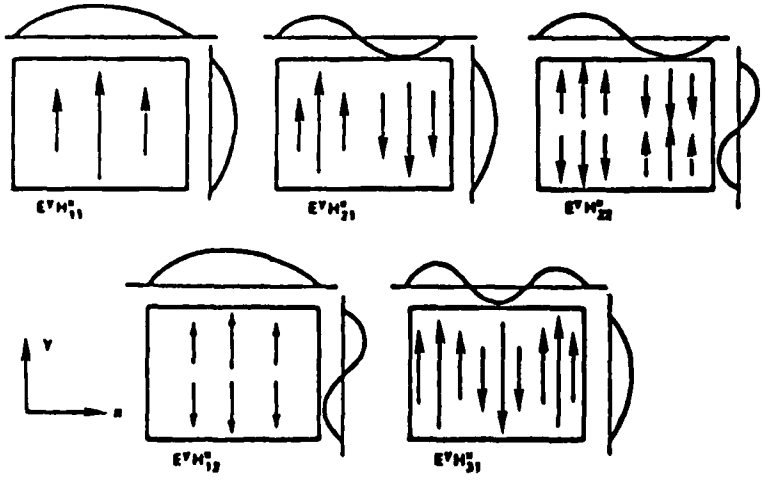

COUPLED-OSCILLATOR ANALOGY

OPTICAL CAVITIES

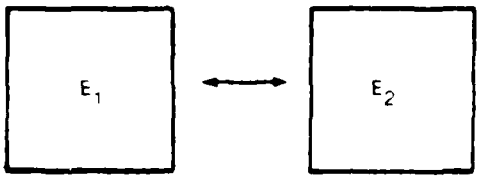

PENDULUMS

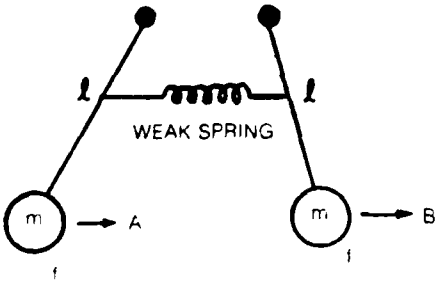

- ASSUMPTIONS:
  - COUPLING IS WEAK
  - OSCILLATIONS ARE NEARLY INDEPENDENT
  - AMPLITUDES & PHASES VARY SLOWLY

- CONSEQUENCES:
  - TWO INDEPENDENT UNCOUPLED OSCILLATIONS ➡ TWO COUPLED MODES
  - EACH MODE HAS A UNIQUE
    - FREQUENCY
    - SET OF AMPLITUDES & PHASES
    - FAR-FIELD INTENSITY
  - PHASE-LOCKING IS POSSIBLE
    - IF FEEDBACK EXISTS

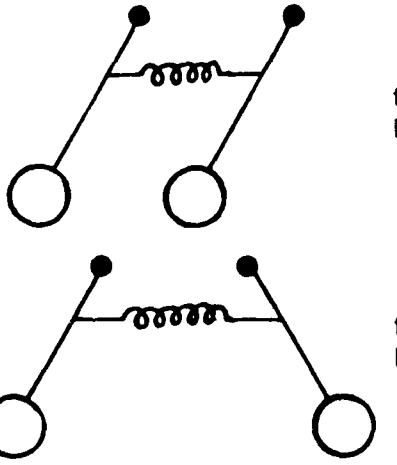

$f' = f$
$B = A$

$f' = f - \Delta f$
$B = -A$

85-3-14-3

A modal analysis for N weakly-coupled lasers arranged in a linear array has been carried out as part of the Coupled Waveguide CO_2 Laser program. Figures 19 through 21 show some of the equations from that analysis, which is based on the model of rectangular waveguides with an infinitely thin partition. The script $\mathcal{E}_n$ is the complex amplitude for the fields in the nth laser in the array. Besides the optical-frequency phase-factor it contains the real, positive amplitude E_n and the real phase (or phase-angle) ϕ_n which are more slowly varying functions of time than the optical phase-factor. The optical interference between different lasers in the array will show up in the relative amplitudes and phases. Basically, the assumed form of the field is inserted into the Maxwell's Equations with a phenomenological term to describe the losses. The right-hand terms, the polarization terms, contain the essential features of the lasing medium, and will be discussed later; they will be ignored in calculating the results of coupling the resonators. The result is a set of coupled-oscillator equations with a coupling arising from the unknown true field in the gap. The best one can do with the coupling term is to approximate it phenomenologically as shown (for one pair of lasers) at the top of Fig. 21. The unknown parameter M is the coupling coefficient. Capital omega is the lowest-order-mode resonator frequency of the lasers (they have all been made equal for the moment) and capital gamma, with the same dimensions as omega, is the amplitude decay parameter due to losses; the polarization (laser) terms have been dropped. The form of the coupling term is based on linearity and symmetry, and is perfectly general. Note that when the fields are opposite and equal, the coupling term vanishes.

There are two 'normal modes', or 'supermodes', for a pair of weakly-coupled resonators. Their frequencies (ω) are shown in the two boxes in Fig. 21, together with their symmetries. Notice that 2M is the frequency shift of the symmetric mode (assuming the coupling M is small compared to Ω), and that there is no frequency shift for the anti-symmetric mode. These results are generalized to a linear array of N lasers in the formulas at the bottom of Fig. 21. The subscript n stands for the nth laser in the array. The superscript m is used to number the supermodes. In this presentation, m=1 is always the symmetric mode. This is the one in which all of the lasers are in-phase, and is the desired supermode from the point of view of getting the largest intensity on a target in the far-field. Numerical values for the frequencies, amplitudes, and phases are presented in Table 2.2 for N=2,3,4 and 5. The phase-angles are either zero or pi, i.e. the complex amplitudes are real, and either positive or negative. Experimental values for N=2 and 3 are presently available, and will be compared with theory as soon as some further points are discussed.

The far-field intensity patterns have been calculated for some of the supermodes, using the cosine fields in the resonators, and the amplitudes and phases predicted by coupled-mode theory (Table 2). The pattern due to a single channel is shown in Figs. 22a and b. In Fig. 22a, the contours of constant

COUPLED-MODE ANALYSIS

$$E_1(x,y,z,t) = \mathcal{E}_1(t) \cos\frac{\pi y}{2a} \cos\frac{\pi(x+a)}{2a} \sin\beta_1 z$$

$$E_2(x,y,z,t) = \mathcal{E}_2(t) \cos\frac{\pi y}{2a} \cos\frac{\pi(x-a)}{2a} \sin\beta_2 z$$

$$\mathcal{E}_1(t) = E_1(t)e^{-i(\omega t + \phi_1(t))}$$

$$\mathcal{E}_2(t) = E_2(t)e^{-i(\omega t + \phi_2(t))}$$

$$\beta_{1,2} \equiv \frac{n\pi}{L_{1,2}}$$

$$\frac{\partial^2 E_1}{\partial t^2} + 2\Gamma_1 \frac{\partial E_1}{\partial t} - c^2\nabla^2 E_1 = -\frac{1}{\varepsilon_o}\frac{\partial^2 P_1}{\partial t^2}$$

$$\frac{\partial^2 E_2}{\partial t^2} + 2\Gamma_2 \frac{\partial E_2}{\partial t} - c^2\nabla^2 E_2 = -\frac{1}{\varepsilon_o}\frac{\partial^2 P_2}{\partial t^2}$$

$$\mathcal{P}_1(t) \equiv \frac{2}{a^2 L}\int_{-2a}^{o} dx \int_{-a}^{a} dy \int_{o}^{L_1} P_1(x,y,z,t) \cos\frac{\pi(x+a)}{2a} \cos\frac{\pi y}{2a} \sin\beta_1 z dz$$

85-3-14-4

COUPLED-MODE EQUATIONS

$$\ddot{\mathcal{E}}_1 + 2\Gamma\dot{\mathcal{E}} + \left(\beta_1^2 c^2 + 2\left(\frac{\pi c}{2a}\right)^2\right)\mathcal{E}_1 - \left(\frac{\pi c^2}{a^3 L_1}\right)\int_{-a}^{a}\int_{o}^{L_1} E_1(o,y,z,t)\cos\frac{\pi y}{2a}\sin\beta_1 z\,dy\,dz$$

$$= -\frac{1}{\varepsilon_o}\ddot{\mathcal{P}}_1(t)$$

$$\ddot{\mathcal{E}}_2 + 2\Gamma\dot{\mathcal{E}}_2 + \left(\beta_2^2 c^2 + 2\left(\frac{\pi c}{2a}\right)^2\right)\mathcal{E}_2 - \frac{\pi c^2}{a^3 L_2}\int_{a-d}^{a}\int_{o}^{L_2} E_2(o,y,z,t)\cos\frac{\pi y}{2a}\sin\beta_2 z\,dy\,dz$$

$$= -\frac{1}{\varepsilon_o}\ddot{\mathcal{P}}_2(t)$$

$$E_1(o,y,z,t) = E_2(o,y,z,t) = E(o,y,z,t)$$

$$\Omega_{1,2}^2 = \beta_{1,2}^2 c^2 + 2\left(\frac{\pi c}{2a}\right)^2$$

NORMAL MODES OF RESONATORS

$$\ddot{\mathcal{E}}_1 + 2\,\Gamma\,\dot{\mathcal{E}}_1 + \Omega^2\mathcal{E}_1 - 2\Omega M\,(\mathcal{E}_1 + \mathcal{E}_2) = 0$$

$$\ddot{\mathcal{E}}_2 + 2\,\Gamma\,\dot{\mathcal{E}}_2 + \Omega^2\mathcal{E}_2 - 2\Omega M\,(\mathcal{E}_1 + \mathcal{E}_2) = 0$$

$$\mathcal{E}_+ = \mathcal{E}_1 + \mathcal{E}_2$$

$$\ddot{\mathcal{E}}_+ + 2\,\Gamma\,\dot{\mathcal{E}}_+ + \Omega^2\mathcal{E}_+ - 4\Omega M\,\mathcal{E}_+ = 0$$

$$\omega_+ = (\Omega^2 - 4\Omega M)^{1/2} = \Omega - 2M$$

$$\mathcal{E}_- = \mathcal{E}_1 - \mathcal{E}_2$$

$$\ddot{\mathcal{E}}_- + 2\,\Gamma\,\dot{\mathcal{E}}_- + \Omega^2\mathcal{E}_- = 0$$

$$\omega_- = \Omega$$

N RESONATORS:

$$\mathcal{E}_n^{(m)} = e^{-i\omega_m t}\,\sin\frac{(2n-1)m\pi}{2n}$$

$$\omega_m = \Omega - 2M\left(1 + \cos\frac{m\pi}{N}\right)$$

versus antisymmetric mode has to be sought in some other effects which have not yet been identified. Such other effects will naturally be expected to play a role in the N=3 case. Future theoretical and experimental efforts will be directed towards identifying and quantifying these unknown effects.

Figure 27 presents a comparison of the ratios of peak intensities in the phased locked (c=coherent) and unlocked (i=incoherent) states as measured and as predicted from the model described above. The comparison is not totally straightforward because, as discussed above, the coupled-mode equations have not been solved with the laser effects included. The earlier measurements for N=2 and N=3 were made at a range of 2 meters from the ouput aperture. A few later measurements were made at a range of 5.8 meters, for N=2 only. The ideal arrangement requires the measurements to be performed well into the so-called 'far-field', i.e., the Fraunhoffer diffraction region, since in this region the intensity distribution has attained its asymptotic profile. The Rayleigh Range, R_R, is a measure of the distance at which the transition from 'near-field' to 'far-field' takes place. It is not precisely defined, but is nominally given by the formula shown in Fig. 27, where D=Nd is the total width of an N element array, and d=2a+s is the distance between centers of neighboring elements. For N=1, N=2, and N=3 its values are 0.74 m, 2.95 m, and 6.63 m, respectively, using the values a=0.1143 cm (45 mils) and s=0.0508 cm (20 mils). Thus, the later N=2 beam profile measurements were performed well into the farfield, but the N=3 measurements were not. A major change in the experimental arrangement will be required to measure beam profile in the far-field for N=3 and greater. It might be pointed out that diffraction theory can predict the results of measurements in the near-field, so that a comparison of experiment and theory is possible in principle with the available data. However, near-field on-axis calculation are quite sensitive to the details of the electric field distribution in the laser output plane, and are probably not worth the considerable extra effort that they would require. In addition, as pointed out in the experimental discussion, the detector aperture size was too large for a good profile measurement at the 2.0 m range; a broad average at the peak was measured. The profile measurement at the 5.8 m range has sufficient resolution for our purposes. However the problem of asymmetry in the profile needs to be resolved before the measurement of on-axis intensity can be considered to be complete.

If A1, A2, and A3 are the three (complex) amplitudes, i.e. the same as E1, E2, and E3, but with the phase (sign) included, then the following relations hold:

QUANTITY	in STATE	is proportional to
Near-Field Power (Pi)	UNLOCKED	$(A1)^2 + (A2)^2 + (A3)^2$
Near-Field Power (Pc)	LOCKED	same
Far-Field Intensity (Ii)	UNLOCKED	same
Far-Field Intensity (Ic)	LOCKED	$(A1 + A2 + A3)^2$

FIG. 26b

3-LASER BEAM PROFILE

m = 3 (W/PHASE REVERSAL): 1, 1, 1

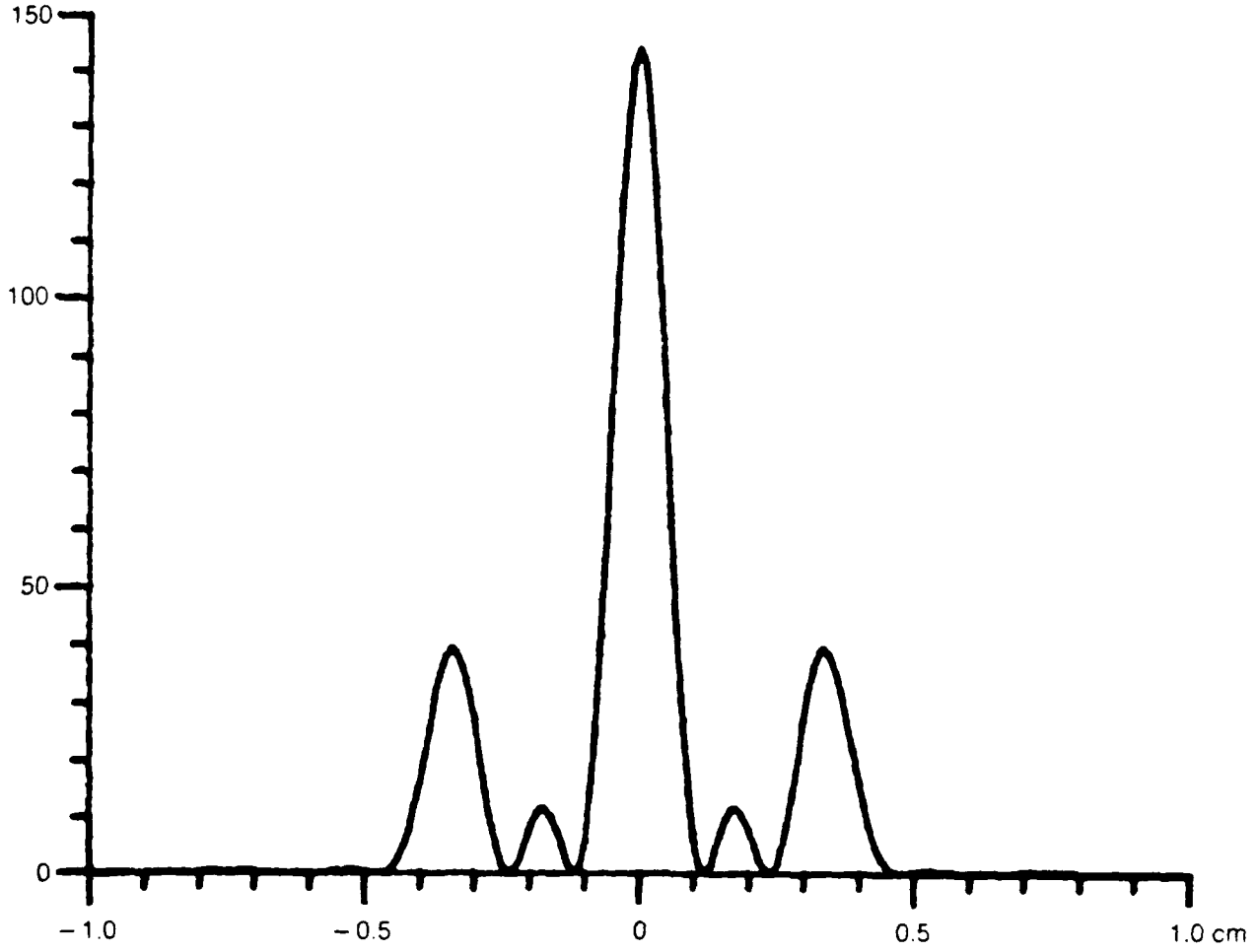

85-3-14-18

FIG. 26a

3-LASER BEAM CONTOURS

m = 3 (W/PHASE REVERSAL): 1, 1, 1

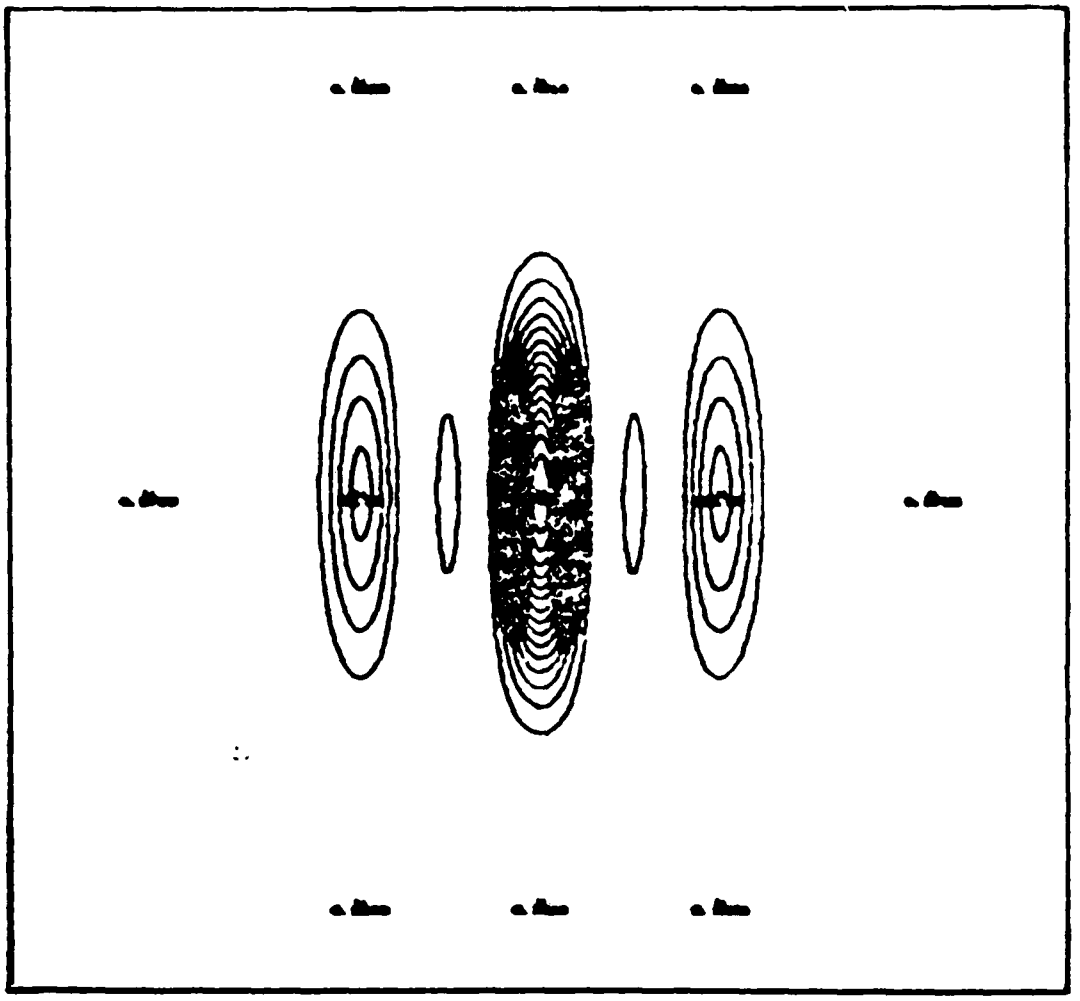

−1

1 cm

85-3-14-17

FIG. 25b

3-LASER BEAM PROFILE

$m = 3: 1, -1, 1$

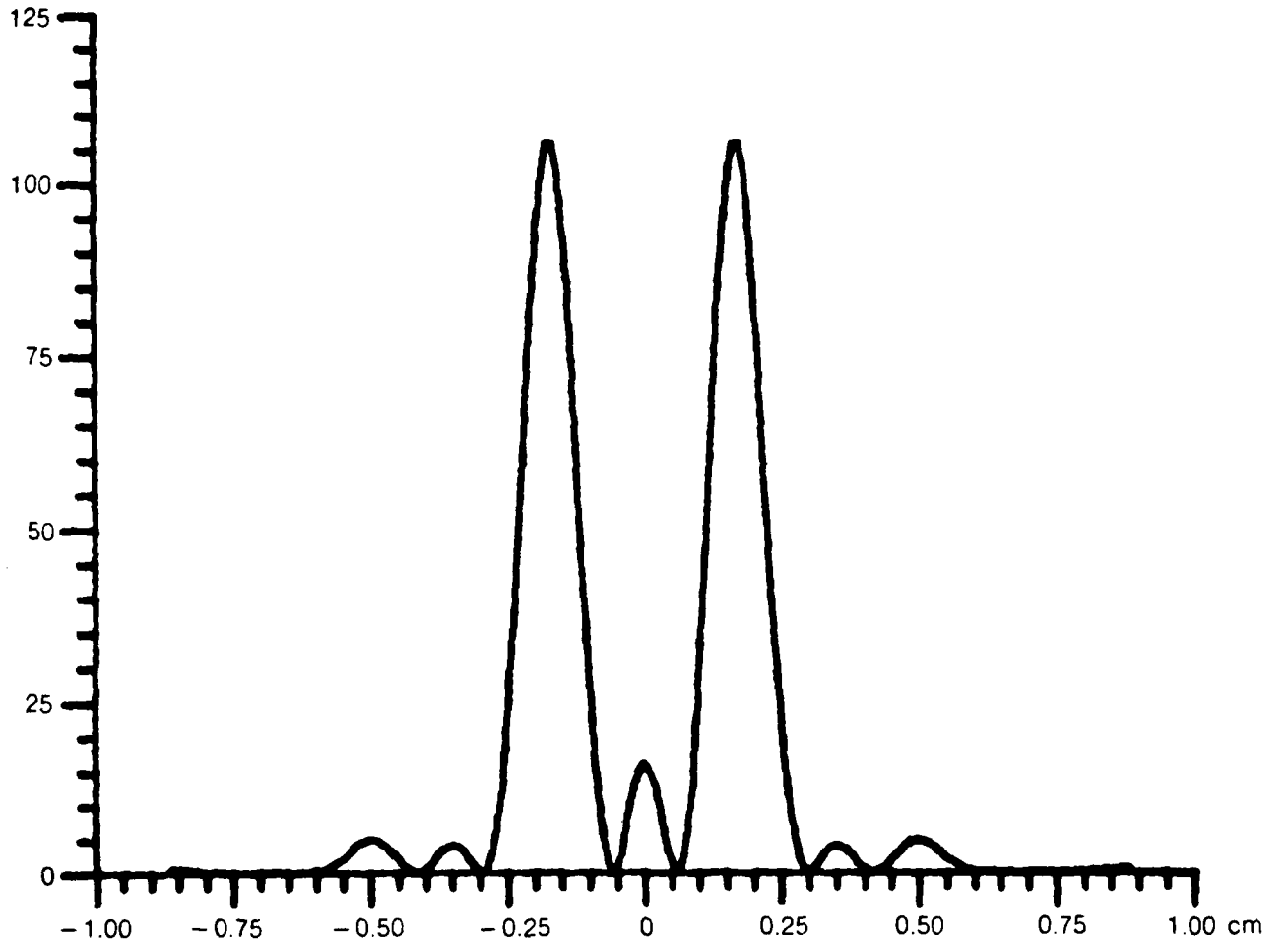

85-3-14-16

FIG. 25a

3-LASER BEAM CONTOURS

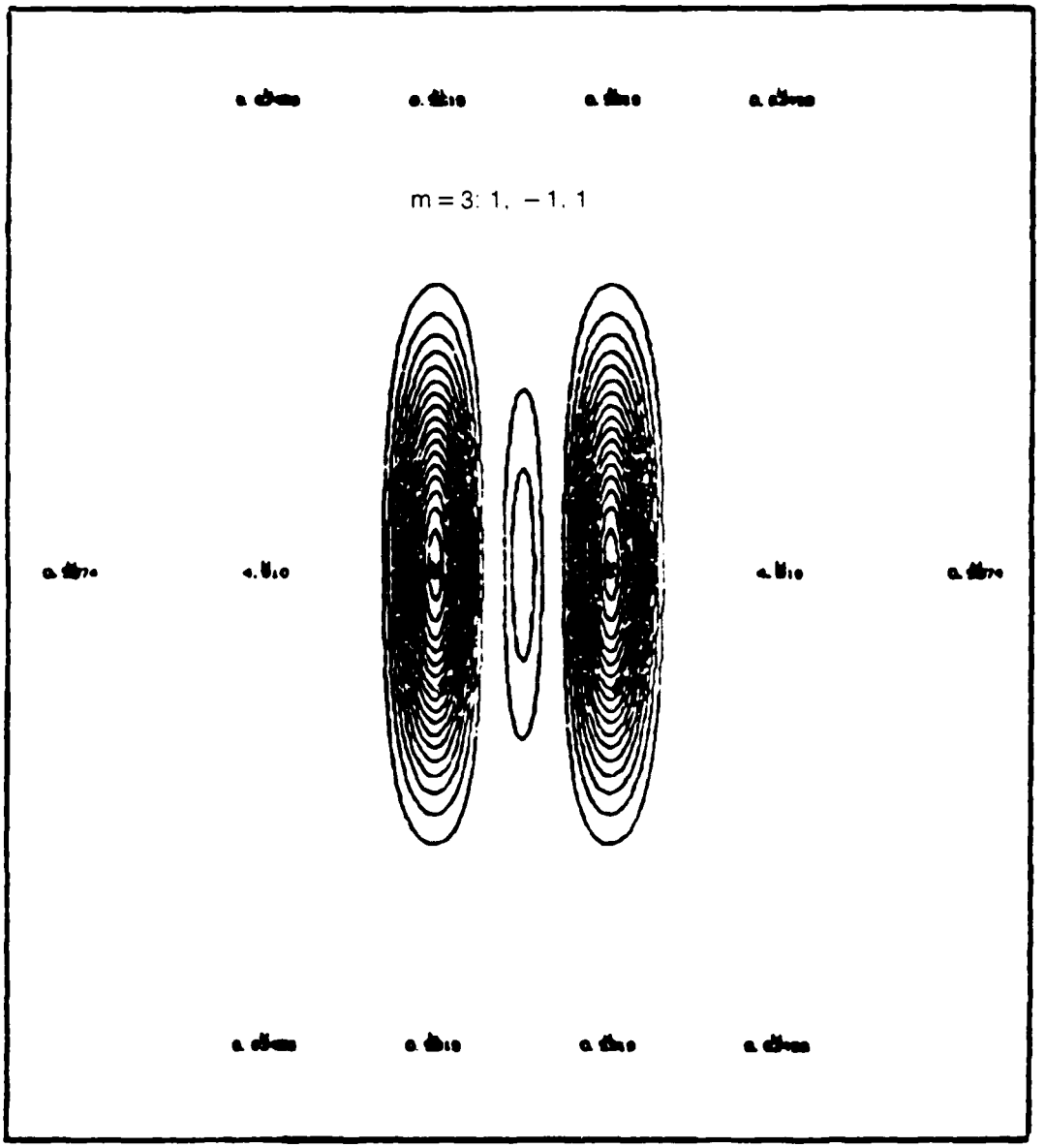

85-3-14-15

FIG. 24b

3-LASER BEAM PROFILE

$m = 2: \sqrt{3}/2,\ 0,\ -\sqrt{3}/2$

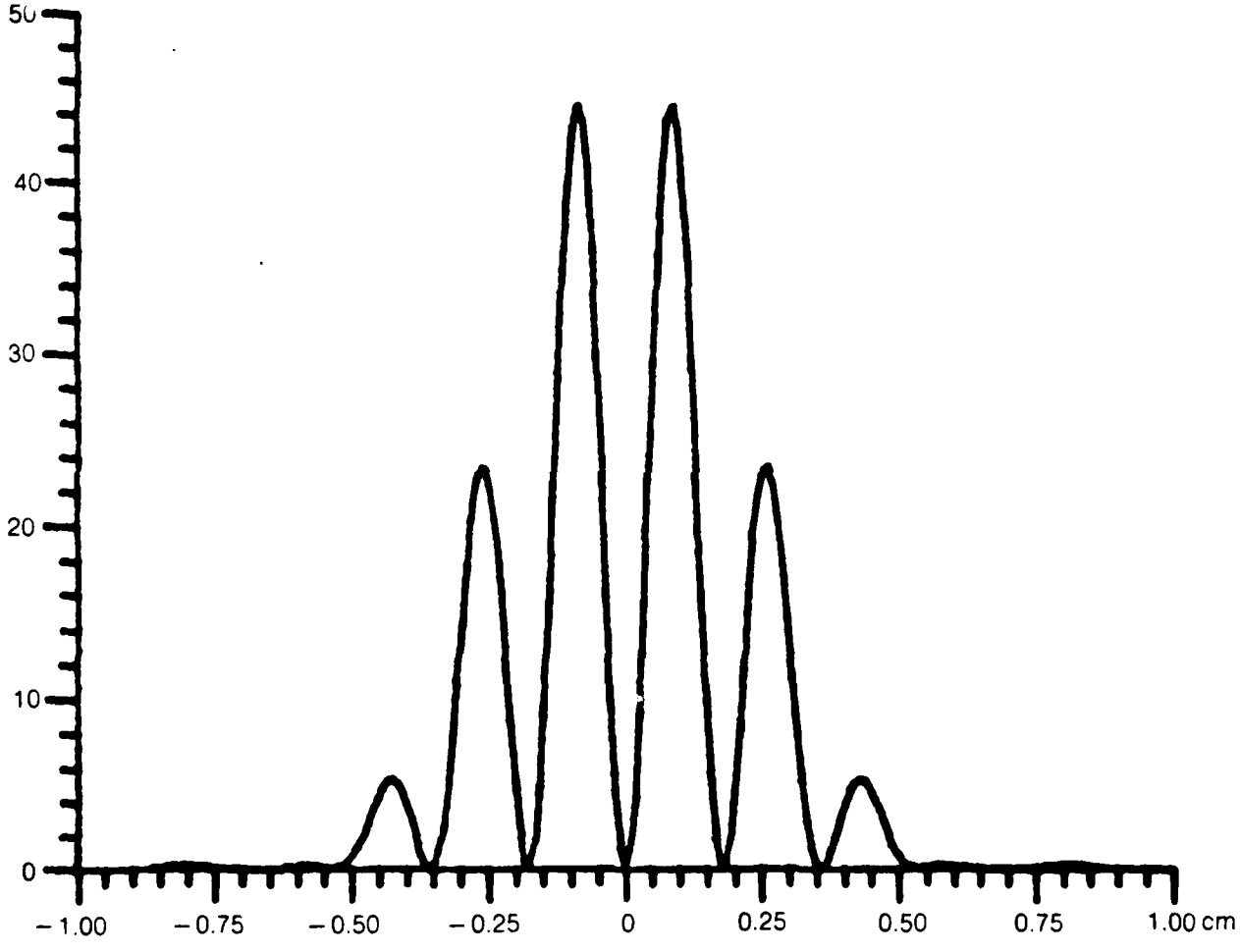

85-3-14-14

3-LASER BEAM CONTOURS

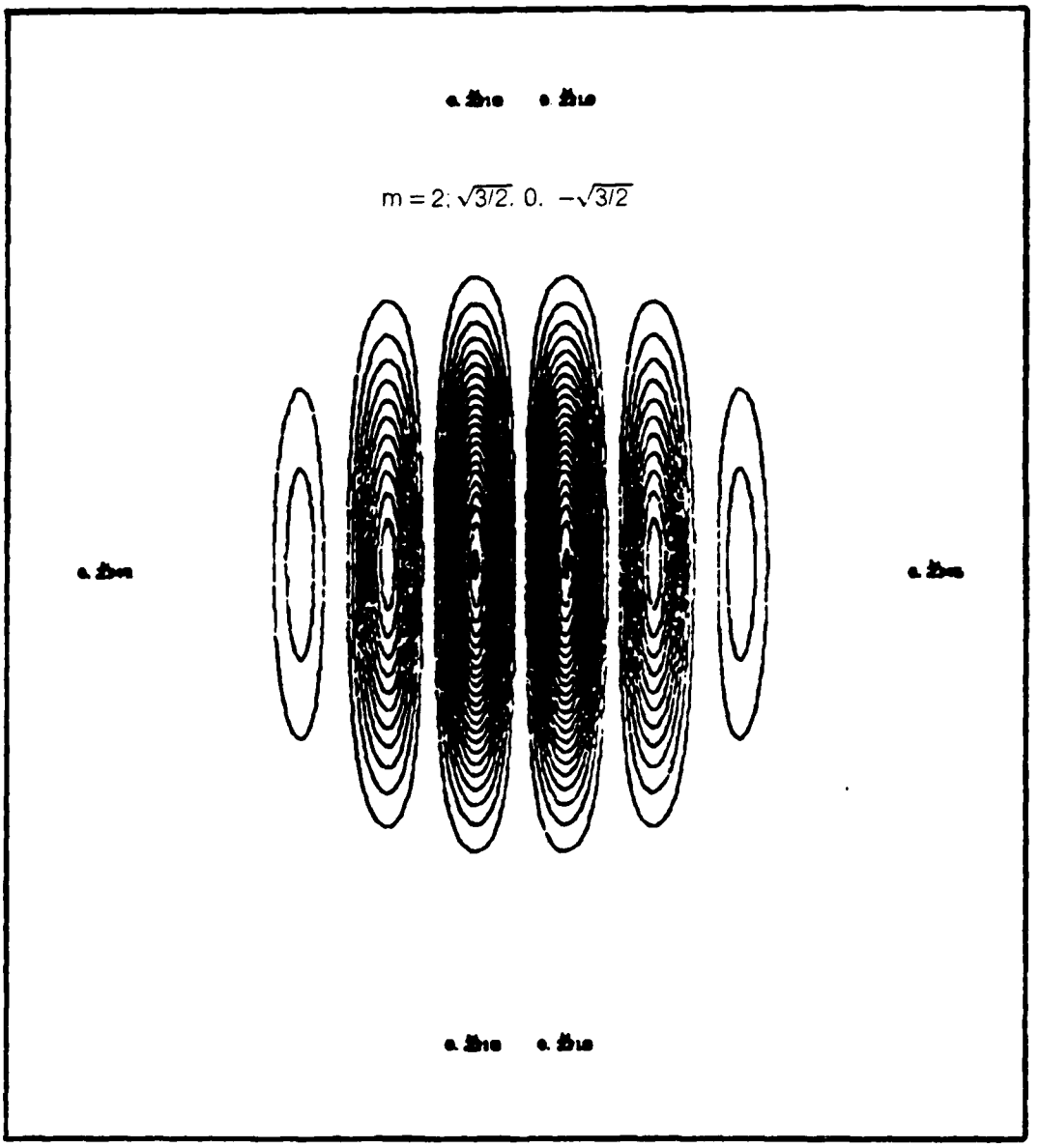

85-3-14-13

3-LASER BEAM PROFILE

m = 1 (SYMMETRIC MODE): 1/2, 1, 1/2

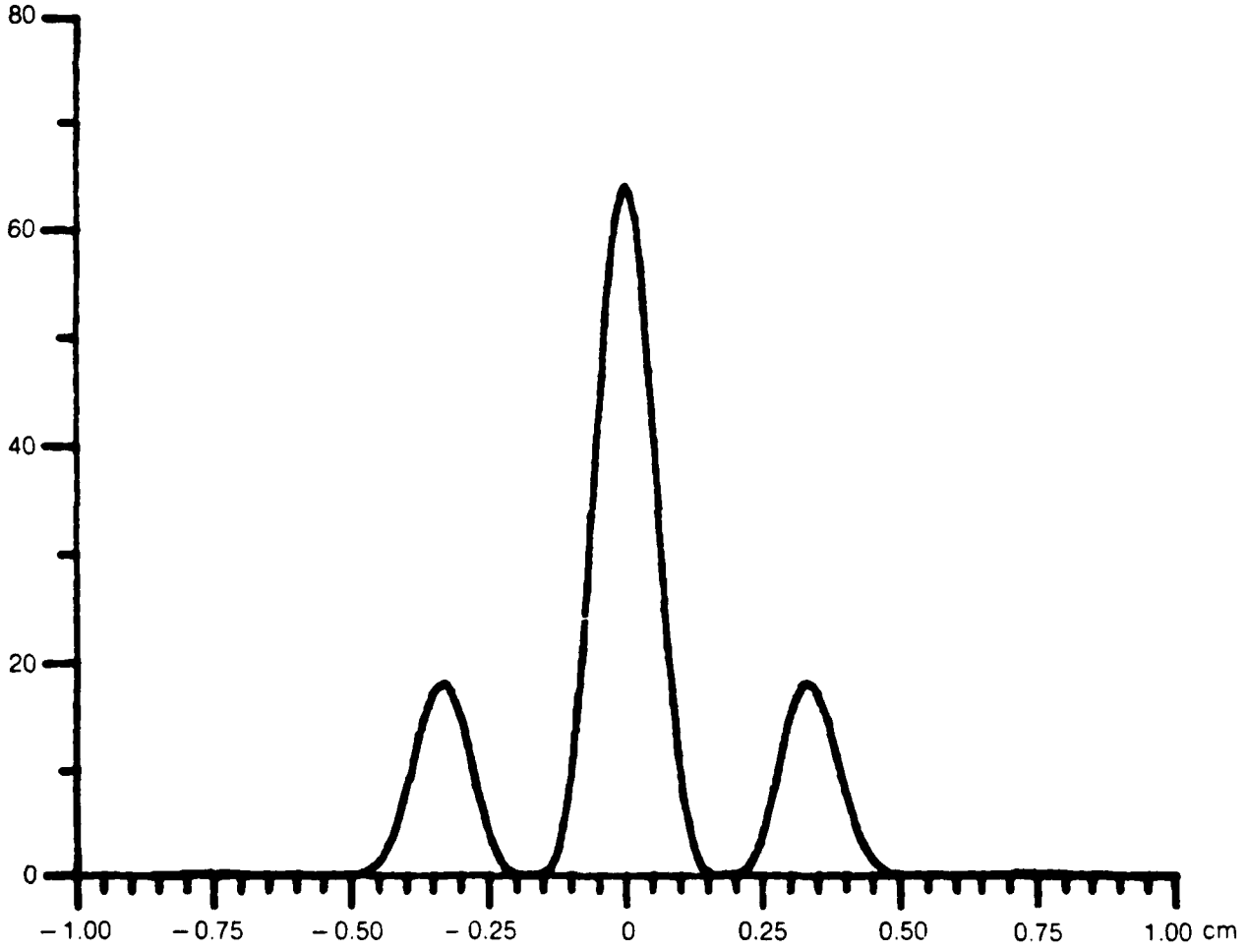

85-3-14-12

3-LASER BEAM CONTOURS

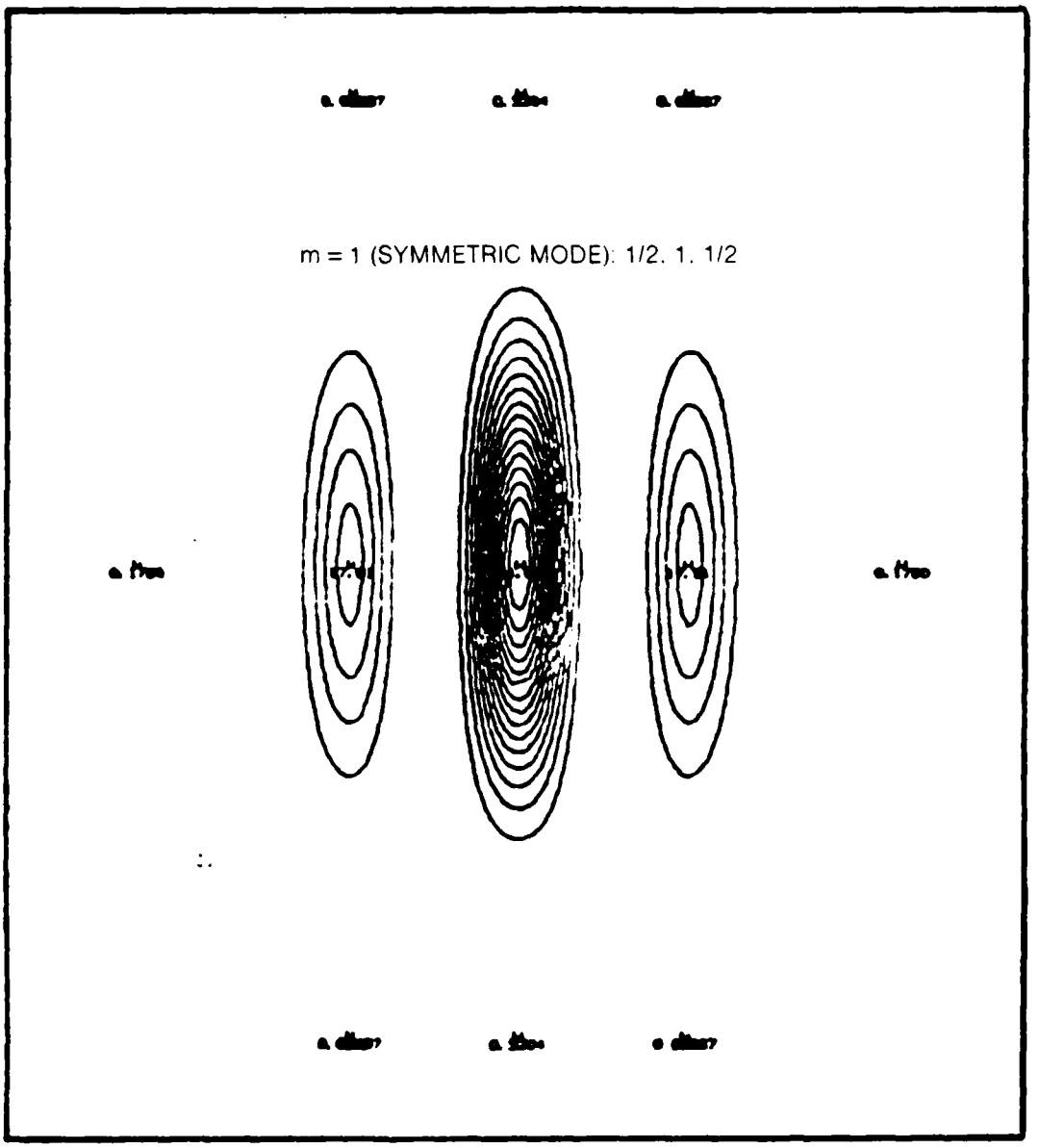

85–3–14–11

intensity have been drawn. The full range of intensities, from maximum to minimum (essentially zero), has been divided into 16 equal intervals, and one contour has been assigned to each division. In Fig. 22b, a single intensity profile through the center of the beam pattern is presented. Figures 23a and b, 24a and b, 25a and b, and 26a and b have a similar meaning, and are drawn to the same horizontal scale, for the N=3 case. The intensity profiles are taken parallel to the linear array. The vertical axes are not drawn to the same scale. The experimentally measured intensity profile for N=3 is shown in Fig. 14. It has the general shape of the theoretical profile for the symmetric mode (m=1, Fig. 23), but is somewhat unsymmetric. It clearly is very different from either of the other non-symmetric modes (m=2, Fig. 24b, and m=3, Fig. 25b). Figures 26a and b do not represent a predicted mode, but will be discussed below.

The symmetric (m=1) mode for N=3 has the three complex amplitudes: (A1,A2,A3)=(1/2,1,1/2). Somewhat surprisingly, they are not equal in magnitude as they are in phase. The intensities (I1,I2,I3) of the three resonator fields are proportional to the squares of the amplitudes, and so are in proportion: (1/4,1,1/4). This result was derived for coupled resonators, not for coupled lasers, but is independent of the coupling coefficient M so long as M is small. For equal lasers one would naturally expect that when their phases are not locked-up their output intensities would be equal: (1,1,1); and therefore that when locked in-phase the magnitudes of their amplitudes would be equal: (E1,E2,E3)=(1,1,1). The linear terms in the coupled-mode equations are tending to drive the laser amplitudes to the ratios: (1/2,1,1/2); while the nonlinear terms may be expected to drive the laser amplitudes towards equality: (1,1,1). Figures 26a and b are intended to show the contours and profiles if this equal-amplitude 'mode' were obtainable.

Now, the m=3 mode is predicted to have equal amplitudes, but not all equal phases: (1,-1,1). We recognize that this mode is more consistent with our expectations for equal lasers than the symmetric mode, and therefore may tend to be preferred when the system of lasers locks-up. One could get the good far-field properties of the equal-amplitude 'mode' by reversing the phase of the middle laser external to the laser, assuming that this was practical to do. Conversely, one could adjust the gains or the losses of the three lasers so that the laser amplitudes would be consistent with the in-phase mode, and thereby increase the preference for it and avoid the need for an external phase-reversal. Experimentally, the 3-channel device does lock-up in the symmetric mode without any gain adjustments being required. Furthermore, the power in the locked-up state is not much below the power in the unlocked state.

We have not yet discussed the N=2 case. The coupled-resonator predictions are for two modes BOTH of which have the same intensity in the two resonators. Thus both are consistent with equal lasers, and the preference for symmetric

FIG. 22b

1-LASER BEAM PROFILE

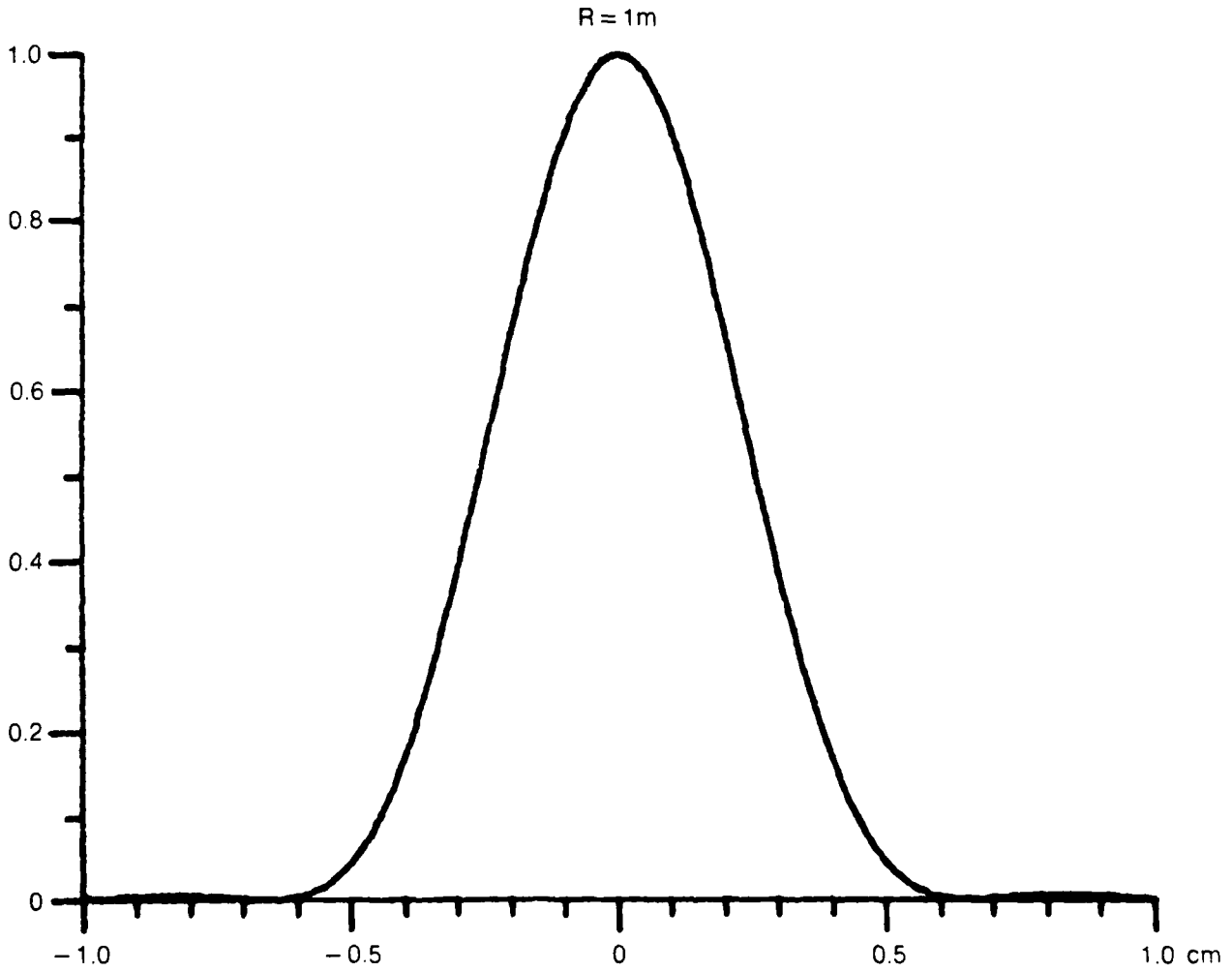

85-3-14-10

1-LASER BEAM CONTOURS

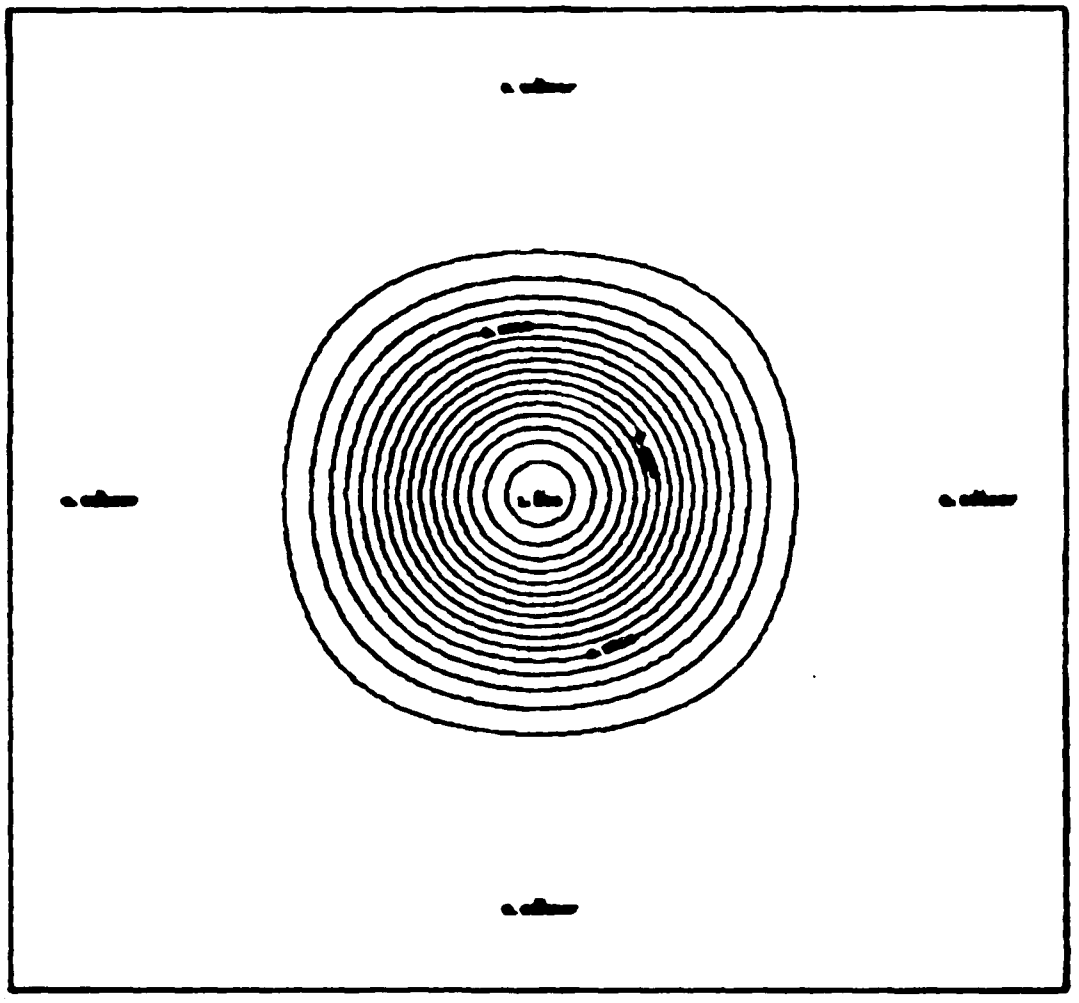

85-3-14-9

TABLE 2 (CONT)
FREQUENCIES AND AMPLITUDES OF NORMAL MODES OF N WAVEGUIDES COUPLED IN LINEAR ARRAYS

N=5	m=1	2	3	4	5
ω_m	$\Omega-3.618M$	$\Omega-2.618M$	$\Omega-1.382M$	$\Omega-.382M$	Ω
$E_1^{(m)}$	.3090	.5878	.8090	.9511	1
$E_2^{(m)}$	.8090	.9511	.3090	-.5878	-1
$E_3^{(m)}$	1.0	0	-1.0	0	1
$E_4^{(m)}$	.8090	-.9511	.3090	.5878	-1
$E_5^{(m)}$	.3090	-.5878	.8090	-.9511	1

85-3-14-8

TABLE 2
FREQUENCIES AND AMPLITUDES OF NORMAL MODES OF N WAVEGUIDES COUPLED IN LINEAR ARRAYS

N=2	m=1	2
ω_m	$\Omega-2M$	Ω
$E_1^{(m)}$	$\sqrt{2}/2$	1
$E_2^{(m)}$	$\sqrt{2}/2$	-1

N=3	m=1	2	3
ω_m	$\Omega-3M$	$\Omega-M$	Ω
$E_1^{(m)}$	1/2	$\sqrt{3}/2$	1
$E_2^{(m)}$	1	0	-1
$E_3^{(m)}$	1/2	$-\sqrt{3}/2$	1

N=4	m=1	2	3	4
ω_m	$\Omega-(2+\sqrt{2})M$	$\Omega-2M$	$\Omega-(2-\sqrt{2})M$	Ω
$E_1^{(m)}$	.3827	$\sqrt{2}/2$	.9239	1
$E_2^{(m)}$	.9239	$\sqrt{2}/2$	-.3827	-1
$E_3^{(m)}$	.9239	$-\sqrt{2}/2$	-.3287	1
$E_4^{(m)}$	.3827	$-\sqrt{2}/2$	.9239	-1

85-3-14-7

FAR-FIELD ON-AXIS INTENSITY RATIO

COHERENT/INCOHERENT (SYMMETRIC MODE)

RAYLEIGH RANGE: $R_R \approx N^2(2s)^2/\lambda \approx N^2\ (2.8\ mm)^2/10.6\mu m = 0.74\ N^2\ m$

	I (COHERENT)/I (COHERENT)	
N = 2 (RAYLEIGH RANGE = 3.0 m)	THEORY	EXPERIMENT
EQUAL-AMPLITUDE/COUPLED-MODE	RANGE = 2.0 m	5.8 m
$I\ (inc) = (1)^2 + (1)^2 = 2$ $I\ (coh) = (1 + 1)^2 = 4$	2 1.7	2.2
N = 3 (RAYLEIGH RANGE = 6.7 m)	THEORY	EXPERIMENT
(A) EQUAL-AMPLITUDE	RANGE = 2.0 m	
$I\ (inc) = (1)^2 + (1)^2 + (1)^2 = 3$ $I\ (coh) = (1 + 1 + 1)^2 = 9$	3 1.8 NOT CONSISTENT WITH COUPLED-MODE THEORY	
(B) COUPLED-MODE	1.33	
$I\ (inc) = (1)^2 + (1)^2 + (1)^2 = 3$ $I\ (coh) = (1/2 + 1 + 1/2)^2 = 4$	NOT CONSISTENT WITH EQUAL POWERS (EXPT)	
(C) COUPLED-MODE. ENHANCED POWER	2.67	
$I\ (inc) = (1)^2 + (1)^2 + (1)^2 = 3$ $I\ (coh) = 2\ (1/2 + 1 + 1/2)^2 = 8$	NO THEORETICAL BASIS FOR ASSUMPTION	

85-7-41-1

There is little or no ambiguity in how to interpret the experimental results for the ratio of the locked on-axis intensity to the un-locked on-axis intensity for N=2. The coupled-mode predictions of equal amplitudes is consistent with assuming that the two channels have equal gain and equal output power. This assumption has been tested against the coupled-mode equations for phase-locking with laser gain terms included (see Fig. 28), and found to be valid. However, the unlocked case has not yet been studied, although it seems plausible to assume that the average gain and power will be the same as in the locked case, as experiments seem to confirm. Thus, the ratio of phase-locked (coherent) to phase-unlocked (incoherent) on-axis intensity is expected to equal 2 (see Fig. 27). The best measurement to date is roughly in agreement with this expectation. By contrast, as already discussed, the N=3 situation is ambiguous because the nonlinear terms have not been included in the solution. In order to gain an idea of what the theoretical solution might indicate, three possibilities are considered. In the first, we use the simple-minded solution (A1,A2,A3)=(1,1,1) which is consistent with the near equality of locked and unlocked powers; however, the predicted intensity ratio is much higher than observed. In the second, we use the coupled-mode theory symmetric resonator mode (m=1) solution (1/2,1,1/2) in the locked state, and the equal lasing solution (1,1,1) in the unlocked state; but this is not consistent with the power equality, and is again in poor agreement with the intensity ratio. In the third, we use the same solutions as for the second, but we arbitrarily raise the overall power level in the locked state by a factor of 2 to get agreement with power equality; this is equivalent to using the solution $(\sqrt{2}/2,\sqrt{2},\sqrt{2}/2)$ in the locked state, but still does not explain the intensity ratio. Clearly, further analysis and further experimentation is required to understand how the lasers are locking-up.

3.3 Phase-Locking

The coupled-mode theory equations, modified by the presence of a lasing medium, are exhibited in Fig. 28. The polarization term is proportional to the electric field, but the saturable gain factor f_i depends on the electric field through the intensity (which is responsible for saturation of the gain). Some definitions are: γ_{ab} is the mean value of the upper and lower lasing level life-times; γ is the homogeneous line-width of the gain line; $\xi=(\omega-\omega_0)/\gamma$ is a dimensionless optical frequency (ω) relative to the center of the gain line (ω_0); $L(\xi)=1/(1+\xi^2)$ is the Lorentzian line-shape factor; p is the dipole matrix element of the laser transition (related to the spontaneous life-time); and h is Planck's constant. The full equation was reduced to a first-order differential equation because the electric-field complex-amplitude varies slowly in time compared to the optical phase. The notations and conventions and simplifications closely follow the usages in Ref. 6.

INCLUSION OF LASER GAIN

$$\ddot{\mathcal{E}}_j + 2\,\Gamma\dot{\mathcal{E}}_j + \Omega_j^2\mathcal{E}_j - 2\Omega_j M\,(\mathcal{E}_j + \mathcal{E}_i) = -\frac{1}{\epsilon_o}\ddot{\mathcal{P}}_j$$

$$j = 1,2 \quad i = 2,1$$

$$\ddot{\mathcal{P}}_j(t) \approx -\omega^2\mathcal{P}_j(t)$$

$$\ddot{\mathcal{E}}_j + \Omega_j^2\mathcal{E}_j = (-\omega^2\mathcal{E}_j - 2i\omega\dot{\mathcal{E}}_j + \Omega^2\mathcal{E}_j) \approx -2i\omega\,(\dot{\mathcal{E}}_j + i\Omega\mathcal{E}_j)$$

$$\boxed{\dot{\mathcal{E}}_j + \Gamma\mathcal{E}_j + i(\Omega_j - M)\,\mathcal{E}_j - iM\mathcal{E}_i = \frac{i\omega}{2\epsilon_o}\mathcal{P}_j}$$

$$j = 1,2 \;:\; i = 2,1$$

$$\mathcal{P}_j(t) = \frac{2\epsilon_o}{\omega}\,(\xi - i)\,f(\xi, I_j)\,\mathcal{E}_j(t)$$

$$f_j(\xi, I_j) \equiv \frac{\gamma}{\gamma_{ab}}\frac{\bar{N}_j}{N_T}\frac{\Gamma}{I_j}\left\{1 - (1 + 2\,\frac{\gamma_{ab}}{\gamma}\,I_j\,L(\xi))^{-1/2}\right\}$$

$$I_j \equiv p^2E_j^2/2h^2\gamma_a\gamma_b$$

$$\boxed{\dot{\mathcal{E}}_j + (\Gamma + i\,(\Omega_j - M))\,\mathcal{E}_j - i\,M\,\mathcal{E}_i = (1 + i\xi)\,f_i(\xi, I_j)\,\mathcal{E}_j}$$

$$j = 1,2 \;;\; i = 2,1$$

85-3-14-20

The phase-locked states are found by asking for the steady-state (time-independent) solutions of these equations. The equations for N lasers, written out in terms of E_n and $_n$, are exhibited in Fig. 29. For N equal resonator frequencies (i.e for all the laser cavities tuned to the same frequency), but without restricting the laser losses and small signal-gains; and neglecting the small frequency-pulling due to the active medium; it is easily found that the resonator supermodes discussed in Section 3.2 are also the supermodes for the lasers, provided the saturated gain equals the loss separately in each laser (see the last equation on Fig. 29). Since the saturated gain depends on the intensity (which is f xed by the supermode), this means that the small-signal gains of the lasers, or their losses, must be tuned to make these N conditions be true.

Even if the lasers are not adjusted to be unequal in order to match the resonator solutions, there will still be steady-state solutions, but now the phases are not just 0 or . However, these solutions have not been studied in detail, and it is not known if they can explain the observed intensity ratios and power ratios. It is proposed to study these solutions further in the follow-on program. The time-dependent, non-steady-state solutions are more difficult to find, but these are needed also, and will be studied. What we have been calling the 'incoherent' or 'un-locked' solutions are actually the time-dependent solutions.

Another feature of the phase-locked solutions that needs to be studied is their stability as differences between the resonator frequencies are introduced. As discussed in Section 3.1, the locking-range, which is a measure of the tolerance of phase-locking to environmental influences, is determined experimentally by physically introducing length changes in the lasers. Theoretically, the locking-range is determined by calculating those lengths for which the nature of the solution changes from stable to unstable (i.e. growing exponentially when perturbed by small amounts).

3.4 Detailed Mode Calculations

Under a Corporate-funded IR&D program, UTRC sponsored the development of a theoretical model of coupled-cavity modes (no lasing effects included) using exact techniques based on electromagnetic theory and the model geometries. Some results of the Corporate-funded research were applied to the present program to help interpret the experimental results.

COUPLED-MODE EQUATIONS FOR N LASERS

$$\dot{E}_1^{(m)} = (f_1(\xi, I_1) - \Gamma_1)E_1^{(m)} + M E_2^{(m)} \sin(\phi_2^{(m)} - \phi_1^{(m)}) \tag{62a}$$

$$\omega_m + \dot{\phi}_1^{(m)} = \Omega_1 - \xi f_1(\xi, I_1) - M\left\{1 + \frac{E_2^{(m)}}{E_1^{(m)}} \cos(\phi_2^{(m)} - \phi_1^{(m)})\right\} \tag{62b}$$

$$\dot{E}_n^{(m)} = (f_n(\xi, I_n) - \Gamma_n) E_n^{(m)} + M E_{n+1}^{(m)} \sin(\phi_{n+1}^{(m)} - \phi_n^{(m)}) - M E_{n-1}^{(m)} \sin(\phi_n^{(m)} - \phi_{n-1}^{(m)}) \tag{63a}$$

$$\omega_m + \dot{\phi}_n^{(m)} = \Omega_n - \xi f_n(\xi, I_n) - M\left\{2 + \frac{E_{n+1}^{(m)}}{E_n^{(m)}} \cos(\phi_{n+1}^{(m)} - \phi_n^{(m)}) + \frac{E_{n-1}^{(m)}}{E_n^{(m)}} \cos(\phi_{n-1}^{(m)} - \phi_n^{(m)})\right\} \tag{63b}$$

$$\dot{E}_N^{(m)} = (f_N(\xi, I_N) - \Gamma_N) E_N^{(m)} - M E_{N-1}^{(m)} \sin(\phi_N^{(m)} - \phi_{N-1}^{(m)}) \tag{64a}$$

$$\omega_m + \dot{\phi}_N^{(m)} = \Omega_N - \xi f_N(\xi, I_N) - M\left\{1 + \frac{E_{N-1}^{(m)}}{E_N^{(m)}} \cos(\phi_{N-1}^{(m)} - \phi_N^{(m)})\right\} \tag{64b}$$

$$f_n(\xi, I_n^{(m)}) = \Gamma_n \tag{65}$$

85-3-14-21

Normal-Mode Analysis: The contract-funded coupled-waveguide program involved waveguide cross-sections and coupled-waveguide geometries for which there are no exact or approximate closed-form expressions for the characteristic frequencies and electromagnetic field distributions. There are some well-known electromagnetic variational techniques for finding approximate solutions for the frequencies and for the modes of a waveguide. One of these has been modified so as to express the modes of a waveguide with an unusual shape in terms of the well-known modes of waveguides of simpler shape. For example, the modes of a rectangular cross-section guide such as that indicated here are known exactly in some cases (such as perfectly conducting walls) and approximately in other cases (such as dielectric walls). However, the modes of a ridged-waveguide such as that shown in the next diagram are only known in terms of infinite series, the coefficients of which depend on the frequencies of the particular modes. These frequencies, in turn, are hidden in transcendental equations (known as dispersion relations), and usually have to be solved for numerically. The series solution for the ridged-waveguide may be found without resort to variational techniques simply by constructing arbitrary series solutions in the three rectangular regions indicated in the next diagram, and matching these fields at the appropriate boundary lines (indicated by the dots). This method, however, is not suitable for a geometry like the U-shaped cross-section used successfully in a number of the coupled-waveguides. Such a geometry is indicated in the next diagram. It is employed because it has the nice feature that it is easier to fabricate this cross-section with very small spacings between the channels (which means a stronger coupling between the channels).

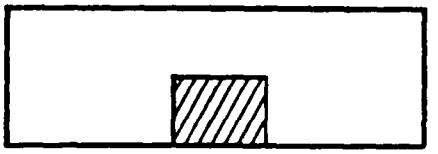

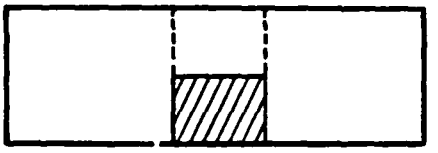

The variational method developed under this Corporate-sponsored research program has not yet been applied to the U-shaped geometry. That task is being proposed as part of the follow-on program. However, the method has been tested on a special example of the ridged-waveguide; namely, for an infinitely thin separator between the channels, as indicated in the last diagram. The results are consistent with the solution achieved in the conventional manner.

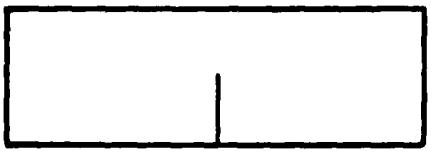

The dispersion relation was solved numerically for the special case in which the gap opening is one-half of the resonator width. The lowest-frequency symmetric mode was found to be -19 MHz below the lowest frequency with no gap. This is one-third of the total difference between zero gap and 100% gap, i.e. no separation at all (-57 MHz). The calculated frequency (-19 MHz) can be used to estimate the coupling constant M, since the coupled-mode theory predicts the frequency shift -2M. Thus $2M/(2\pi) = 19$ MHz, which is also the minimum beat frequency (MBF) between the symmetric and antisymmetric modes of a pair of coupled oscillators. Coupled-mode theory also predicts the beat frequency between the coupled modes when the resonator frequencies are not equal; the formula is given in Fig. 30. Now, because of phase-locking, one cannot experimentally observe the MBF, only the minimum observed beat frequency (MOBF). The latter is the beat frequency for that value of the resonator frequency difference ($\Delta\Omega_L$) at which the transition from unlocked to locked occurs. One has to solve for the locking-range to complete the calculation.

The locking-range was calculated for a related problem involving coupled lasers on another program (Ref. 7). The lasers (which were not waveguide lasers, but were CO_2 lasers) were coupled through a common end-mirror. The locking-range was calculated for several conditions. The locking-range is essentially linear with M (see Fig. 31). For the present program, it is estimated from a Rigrod laser analysis that $\Delta\omega_L$ is approximately 2M also. The result of these various estimates is a predicted MOBF of 27 MHz. This is in fair agreement with the MOBF seen experimentally for the smallest separations (23 MHz) if one realizes that the geometry of the cross-section is different from that used in the detailed mode theory; and that the coupling is probably too large for the coupled-mode theory to be strictly valid. In future work, this calculation will be pursued further. As part of the phase-locking analysis, the locking-range will be calculated for the correct experimental situation, and an attempt will be made to calculate M for the correct geometries.

MINIMUM OBSERVED BEAT FREQUENCY (MOBF)

EXPERIMENTAL

SHAPE	GAP (mils)	SEPARATION (mils)	MOBF (MHz)
	35	20	4.8
	45	20	6.8
	45	10	11.0
	45	0	23.0
	55	−3	23.0
	55	20	13.5
	30	12	1.4

THEORETICAL

OBSERVED LOCKING RANGE
$\Delta\Omega_L$ NOT MEASURED

$\Delta\Omega_L \approx 2M$ (ESTIMATED)

$$\omega_B = \sqrt{(\Delta\Omega)^2 + (2M)^2}$$

$$\omega_{MBF} = 2M = 2\pi\Delta f$$

$$\omega_{MOBF} = \sqrt{(\Delta\Omega)_L^2 + (2M)^2}$$

$$\approx \sqrt{2}\ (2M)$$

$$f_{MOBF} \approx (1.4)(19) = 27\ \text{MHz}$$

85-3-14-22

EXAMPLE OF PHASE-LOCKING-RANGE

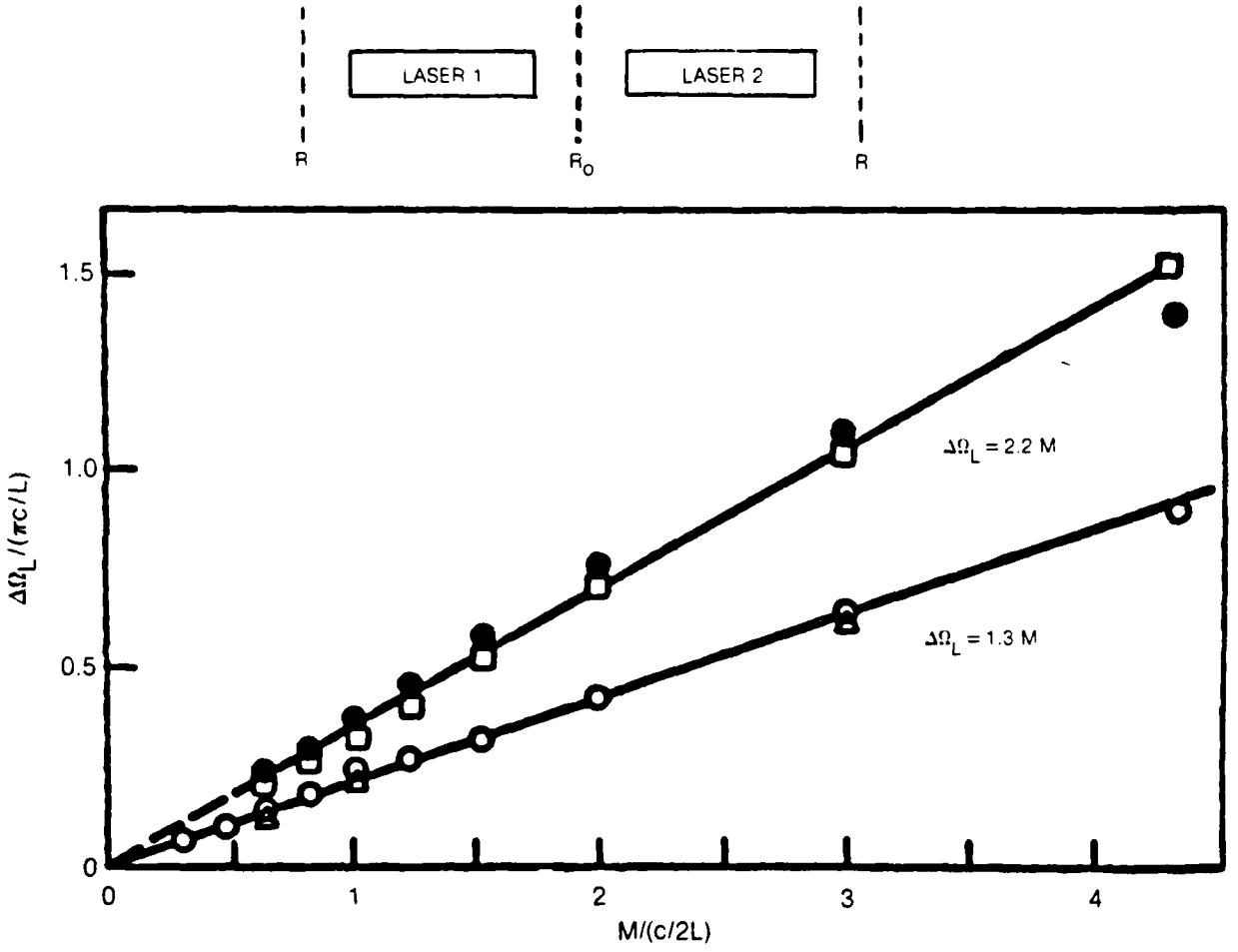

85-3-14-23

4.0 REFERENCES

1. Private communication from A. J. DeMaria to L. A. Newman: Phase Locking of a Large Number of CO_2 Waveguide Lasers for High Power Extraction, October 11, 1982.

2. Private communication from A. J. DeMaria to L. A. Newman: Dielectric Ridged Waveguide Gas Lasers, October 27, 1982.

3. U. S. Patent No. 4,443,877, Uniformly Excited RF Waveguide Laser, April 17, 1984.

4. U. S. Patent No. 4,363,126, Tuned-Circuit RF-Excited Laser, December 7, 1982.

5. J. Degnan: The Waveguide Laser: A Review. Applied Phys., 11, 1-33 (1976).

6. M. Sargent, M. V. Scully and W. E. Lamb, Jr.: Laser Physics, Addison-Wesley, Reading, MA, 1974.

7. W. J. Fader: Theory of Two Coupled Lasers, to be published in IEEE JQE.

END

FILMED

11-85

DTIC